2005

Mass-to-light ratio gradients in early-type galaxy haloes

N. R. Napolitano
M. Capaccioli
Aaron J. Romanowsky, *San Jose State University*
N. G. Douglas
M. R. Merrifield, *University of Nottingham*, et al.

Mass-to-light ratio gradients in early-type galaxy haloes

N. R. Napolitano,[1]* M. Capaccioli,[2,3] A. J. Romanowsky,[4,5] N. G. Douglas,[1]
M. R. Merrifield,[5] K. Kuijken,[1,6] M. Arnaboldi,[7] O. Gerhard[8] and K. C. Freeman[9]

[1]*Kapteyn Astronomical Institute, Postbus 800, 9700 AV Groningen, the Netherlands*
[2]*INAF–Astronomical Observatory of Capodimonte, via Moiariello 16, I-80131 Naples, Italy*
[3]*Department of Physical Sciences, University "Federico II", Naples, Italy*
[4]*Departamento de Física, Universidad de Concepción, Casilla 160-C, Concepción, Chile*
[5]*School of Physics and Astronomy, University of Nottingham, University Park, Nottingham NG7 2RD*
[6]*Leiden Observatory, Niels Bohrweg 2, NL-2333 CA Leiden, the Netherlands*
[7]*INAF–Astronomical Observatory of Pino Torinese, via Osservatorio 20, I-10025 Pino Torinese, Italy*
[8]*Astronomy department, University of Basel, Venusstrasse, Basel, Switzerland*
[9]*RSAA, Mt. Stromlo Observatory, Weston Creek P.O., ACT 2611, Australia*

ABSTRACT

Owing to the fact that the near future should see a rapidly expanding set of probes of the halo masses of individual early-type galaxies, we introduce a convenient parameter for characterizing the halo masses from both observational and theoretical results: $\nabla_\ell \Upsilon$, the logarithmic radial gradient of the mass-to-light ratio. Using halo density profiles from Λ-cold dark matter (CDM) simulations, we derive predictions for this gradient for various galaxy luminosities and star formation efficiencies ϵ_{SF}. As a pilot study, we assemble the available $\nabla_\ell \Upsilon$ data from kinematics in early-type galaxies – representing the first unbiased study of halo masses in a wide range of early-type galaxy luminosities – and find a correlation between luminosity and $\nabla_\ell \Upsilon$, such that the brightest galaxies appear the most dark-matter dominated. We find that the gradients in most of the brightest galaxies may fit in well with the ΛCDM predictions, but that there is also a population of fainter galaxies whose gradients are so low as to imply an unreasonably high star formation efficiency $\epsilon_{SF} > 1$. This difficulty is eased if dark haloes are not assumed to have the standard ΛCDM profiles, but lower central concentrations.

Key words: galaxies: evolution – galaxies: fundamental parameters – galaxies: haloes – galaxies: kinematics and dynamics – dark matter.

1 INTRODUCTION

Spiral galaxies have long been known to show apparent increases in the mass-to-light ratio (M/L) in their outer parts, which was one of the prime factors in discovering the ubiquity of dark matter in the universe (Bosma & van der Kruit 1979; Whitmore, Forbes & Rubin 1988). Current studies of spiral galaxy rotation curves largely focus on the observed radial distribution of the dark matter vis-à-vis the predictions of the current cosmological paradigm, cold dark matter (CDM) with a cosmological constant (ΛCDM). In particular, ΛCDM simulations of galaxy halo formation predict a steep cusp of dark matter in the halo centres (Navarro, Frenk & White 1996, 1997: NFW hereafter; Moore et al. 1999), while many observations of late-type galaxies indicate relatively low central concentrations of dark matter (see Alam, Bullock & Weinberg 2002; Marchesini et al. 2002; de Blok, Bosma & McGaugh 2003; Gentile et al. 2004;

and references therein). It remains to be seen if this discrepancy can be traced to observational problems, to oversimplified predictions of the halo properties (especially with respect to the inclusion of baryonic effects), or to a fundamental failure of the ΛCDM paradigm.

Early-type galaxies (ellipticals and lenticulars) are as numerous as late types, and it is important to see how their dark-matter distributions compare to those of spirals and to theoretical predictions. Historically, the lack of easily interpretable mass tracers like the cold gas in spirals has made it very difficult to map the mass distribution in early types at large distances from their centres. Observations of stellar kinematics from integrated-light spectra are mostly confined within $2R_e$ (where the effective radius R_e encloses half the projected light), which is generally insufficient for establishing the presence of a dark-matter halo (Kronawitter et al. 2000; Magorrian & Ballantyne 2001) – much less for determining its detailed properties. Attempts to constrain the dark-matter content in this way have produced inconsistent results (Gerhard et al. 2001; Borriello, Salucci & Danese 2003; Trujillo, Burkert & Bell 2004; Padmanabhan et al.

* E-mail: nicola@astro.rug.nl

2004; Mamon & Łokas 2004a), demonstrating the difficulties inherent in studying the stellar-dominated regions.

Tracers at larger radius in early-type galaxies are needed, and recent advances in instrumentation have dramatically improved the feasibility of measuring halo masses using planetary nebulae (PNe; Douglas et al. 2002), globular clusters (GCs; Dirsch et al. 2004), gaseous X-ray emission (Matsushita et al. 2002; O'Sullivan & Ponman 2004b), gravitational lensing (Keeton 2001) and extended H I discs (Oosterloo et al. 2002). Such studies have so far ascertained the presence of both massive (Romanowsky & Kochanek 2001; Buote et al. 2002; Napolitano, Arnaboldi & Capaccioli 2002; Côté et al. 2003; Richtler et al. 2004; O'Sullivan & Ponman 2004b; Treu & Koopmans 2004) and weak (Méndez et al. 2001; Romanowsky et al. 2003; Peng, Ford & Freeman 2004) dark haloes. Various attempts have been made using halo tracers to derive generic constraints on dark matter in ellipticals (Bertola et al. 1993; Bahcall, Lubin & Dorman 1995; Danziger 1997; Loewenstein & White 1999), but none of these has used a large, well-defined sample of ellipticals covering a broad range of luminosities. With ongoing observational projects aimed to the study of mass distribution around early-type galaxies using stellar kinematics (SAURON: de Zeeuw et al. 2002; PN.S project: Douglas et al. 2002), strong gravitational lensing (SGL; CLASS: Myers et al. 1995; and LSD: Koopmans & Treu 2002) and X-rays (O'Sullivan & Ponman 2004a,b), we expect to have, in the near future, a much better observational picture of the halo mass distributions in a large representative sample of early-type galaxies.

To prepare for this observational onslaught, in this paper we want to provide a suite of predictions from the ΛCDM theory for halo mass distributions. To gain qualitative insight, we begin with the most basic characterization of a dark-matter halo around a luminous galaxy: the M/L radial gradient. In conjunction with deriving predictions for this gradient, we illustrate the kind of analysis possible with future extensive data sets by comparing the currently available observational results with the model expectations. This approach may be contrasted with the detailed analysis of individual galaxies, where one attempts to decompose the mass distributions into their baryonic and non-baryonic components and then compare these to ΛCDM predictions. Here we are more simply looking at a broad property of the mass profiles which can be statistically analysed. Note that even with detailed analyses, it may never be possible in individual galaxies to unravel all the geometrical and dynamical degeneracies, necessitating a statistical approach such as in this paper in order to interpret the results.

The paper is organized as follows: in Section 2 we introduce the M/L gradient $\nabla_\ell \Upsilon$ as a basic quantity for describing the relative distributions of luminous and dark mass; in Section 3 we present predictions from ΛCDM for $\nabla_\ell \Upsilon$, including its dependence on various galaxy properties; in Section 4 we assemble observational results on $\nabla_\ell \Upsilon$ for a sample of galaxies from the literature, and we test for correlations with other observed properties; in Section 5 we compare the observed and predicted trends in $\nabla_\ell \Upsilon$, and examine the implications for galaxy formation. We draw conclusions in Section 6.

2 THE *M/L* GRADIENT

Aiming for the simplest characterization of the dark-matter content of a galaxy, we could consider the total M/L at some large radius, such as the benchmark quantity Υ_{B5} (*B*-band M/L within 5 R_e) introduced by Romanowsky et al. (2003). This would allow for constructions similar to the Tully–Fisher relations in spiral galaxies,

but in comparing different galaxies, a quantity such as Υ_{B5} is complicated by differences in the stellar luminosities (i.e. in the stellar M/L, Υ_*). Instead, we consider the increase in the M/L with radius relative to its value in the galaxy centre (where it is presumably dominated by Υ_*). This M/L gradient gives us a clearer idea of how much extra mass resides in the halo, and it is computed below.

The M/L gradient is a continuously varying quantity with the (three-dimensional) radius, but its average value between an inner and an outer radius (r_{in}, r_{out}) is given by

$$\frac{\Delta \Upsilon}{\Delta r} = \frac{\Upsilon_{out} - \Upsilon_{in}}{r_{out} - r_{in}} = \frac{\Upsilon_*}{\Delta r}\left[\left(\frac{M_d}{M_*}\right)_{out} - \left(\frac{M_d}{M_*}\right)_{in}\right], \quad (1)$$

where $M_*(r)$ and $M_d(r)$ are respectively the luminous (stellar) and the dark masses enclosed within a certain radius. This is the absolute value of the gradient, but to normalize galaxies of different mass and size to similar scales, we compute

$$\frac{R_e \Delta \Upsilon}{\Upsilon_* \Delta r} = \frac{R_e}{\Delta r}\left[\left(\frac{M_d}{M_*}\right)_{out} - \left(\frac{M_d}{M_*}\right)_{in}\right] \equiv \nabla_\ell \Upsilon. \quad (2)$$

Thus $\nabla_\ell \Upsilon$ is approximately equivalent to the logarithmic gradient of the M/L. The predicted value for $\nabla_\ell \Upsilon$ is the middle expression of equation (2) (also referred to as $\nabla_\ell^{mod} \Upsilon$ hereafter), and is uniquely determined once the mass distributions and measurement radii are adopted (see Section 3). The empirical value is the left expression ($\nabla_\ell^{obs} \Upsilon$, hereafter); in addition to any dynamical modelling uncertainties in $\Delta \Upsilon$, Υ_* is a source of systematic uncertainty (discussed later). Although $\nabla_\ell \Upsilon$ will in principle depend on the location of its measurements ($r_{in}/R_e, r_{out}/R_e$), the ratio $M_d(r)/M_*(r)$ can, to a first approximation, be assumed to vary linearly with the radius (i.e. not to have strong local gradients), such that $\nabla_\ell \Upsilon$ is fairly independent of the measurement radius (we check this for a theoretical model in Sections 3.3 and 3.4; see also Dubinski 1998). This allows us to uniformly compare observational results where the values of ($r_{in}/R_e, r_{out}/R_e$) are rather heterogeneous. Note also that $\nabla_\ell \Upsilon$ is independent of the filter bandpass used for the M/L estimates.

3 PREDICTIONS FROM ΛCDM

We build spherical representations of early-type galaxy mass profiles, using a constant M/L model for the stellar distribution (Section 3.1) plus a ΛCDM model of the dark halo (Section 3.2). We combine these components in Section 3.3. We do not include a diffuse gas component, because we expect its mass inside ∼5R_e to be a small fraction of the stellar mass (we discuss the effect of this assumption in Section 3.4). We derive the predictions for various model parameters in Section 3.4.

3.1 The luminous component

The Hernquist (1990) profile is known to be a fairly accurate representation of the stellar mass distribution in early-type galaxies; in projection, it approximates well the $R^{1/4}$ law of de Vaucouleurs (1948). Assuming Υ_* to be radially constant, the stellar mass density distribution is

$$\rho_*(r) = \frac{M_*}{2\pi} \frac{k\, R_e}{r\, (r + k\, R_e)^3}, \quad (3)$$

where $k \simeq 0.5509$. The cumulative mass profile is

$$M_*(r) = M_* \frac{(r/R_e)^2}{(r/R_e + k)^2}. \quad (4)$$

Thus we have a family of density distributions characterized by two parameters: the total luminous mass, M_*, and the effective

radius R_e. These parameters do not vary arbitrarily in early-type galaxies [as demonstrated by the fundamental plane (FP)] but are correlated by a power law of the form

$$\frac{R_e}{h^{-1} \text{ kpc}} = R_M \left(\frac{M_*}{h^{-1} 10^{11} \text{ M}_\odot} \right)^\alpha. \tag{5}$$

The scatter of the parameters (α, R_M) in equation (5) is an important source of uncertainty which we will address in more detail in later sections. In this section we start drawing predictions for generic early-type galaxies in ΛCDM. For this reason we assume the results from Shen et al. (2003) based on a large statistical sample (about 140 000 galaxies) as a reasonable representation of the size–mass scaling properties of early types.

Shen et al. (2003) found for their SDSS sample of early-type galaxies that $\alpha = 0.56$ and $R_M = 3.6$ ($R_M = 4.17$ for $h = 0.7$), consistent also with the results of Chiosi et al. (1998). Other studies of large samples of early-type galaxies have found mean relations between total luminosity and effective radius of $R_e \propto L^\gamma$, with $\gamma = 0.54$–0.63 (Pahre, Djorgovski & de Carvalho 1998; Bernardi et al. 2003; Mamon & Łokas 2004a), i.e. a slope very similar to the Shen et al. (2003) results under the assumption that Υ_* is constant with M_* (and L). In this case we could take $\alpha = \gamma = 0.6$ as an average value. If this assumption is not true, as suggested by FP studies, then a relation $\Upsilon_* \propto M_*^\beta$ implies $R_e \propto L^\gamma \propto M_*^{(1-\beta)\gamma}$ and $\alpha = (1-\beta)\gamma$. The exponent β depends on the passband and has been found to lie in the range $\beta \sim 0.2$–0.6 (Pahre, Djorgovski & de Carvalho 1995; Gerhard et al. 2001); assuming $\gamma = 0.6$ and an intermediate value of $\beta = 0.3$, we obtain $\alpha = 0.4$. Higher values are found using the $\mu_e - R_e$ relation (Kormendy 1977) and the assumption of homology ($L \propto I_e R_e^2$, where μ_e and I_e are the effective surface brightness in magnitudes and luminosities, respectively). The Kormendy relation $\mu_e \sim 3 \log R_e$ implies $\log I_e \sim -1.2 \log R_e$ and with a bit of algebra, $\gamma = 1.25$, giving $\alpha = 0.9$–1.2 for $\beta = 0$–0.3.

We thus adopt $\alpha = 0.56$ as a characteristic value in equation (5), with $\alpha = 0.4$–1.2 representing the plausible range. Later in the paper, when comparing model predictions with observations, we will check that this size–mass relation is consistent with our galaxy sample (Section 4.2). Note that, besides the relation ($\alpha = 0.56, R_M = 3.6$) for massive galaxies ($M_* > 2 \times 10^{10} \text{ M}_\odot \, h^{-1}$), Shen et al. (2003) also provide a shallower relation ($\alpha = 0.14, R_M = 1.57$) for dwarf ellipticals (dEs).

3.2 The dark component

It is a basic prediction of CDM that visible galaxies are embedded in extended haloes of dark matter. N-body simulations of hierarchical formation in the 'concordance' ΛCDM cosmology ($\Omega_m = 0.3$, $\Omega_\Lambda = 0.7$, $\sigma_8 = 0.9$: NFW; Bullock et al. 2001; Wechsler et al. 2002) produce average dark halo mass profiles of the form

$$\rho_d(r) = \frac{\rho_s}{(r/r_s)(1 + r/r_s)^2}, \tag{6}$$

where r_s is the inner characteristic length-scale, corresponding to the radius where the logarithmic slope of the profile is -2. Equation (6) can be written in terms of the total mass M_d at the virial radius r_{vir} and of the concentration parameter $c_d \equiv r_{vir}/r_s$, i.e.

$$\rho_d(r) = \frac{M_d}{4\pi A(c_d)} \frac{1}{r(1+r)^2}, \tag{7}$$

where $M_d = 4\pi \rho_s r_s^3 A(c_d)$ and

$$A(x) = \ln(1+x) - \frac{x}{1+x}. \tag{8}$$

The cumulative mass profile is then

$$M_d(r) = M_d \frac{A(r/r_s)}{A(c_d)}, \tag{9}$$

where we have followed the notation of Borriello et al. (2003). In principle, NFW profiles are a two-parameter family of density distributions (ρ_s and r_s, or equivalently M_d and c_d).[1] However, a key result of ΛCDM theory is that the halo concentration correlates on average strongly with the virial mass (Bullock et al. 2001; Wechsler et al. 2002), which for a population of haloes at $z = 0$ may be written as[2]

$$c_d(M_{vir}) \simeq 17.1 \left(\frac{M_{vir}}{h^{-1} 10^{11} \text{ M}_\odot} \right)^{-0.125}, \tag{10}$$

where the overdensity of the halo mass relative to the critical density has been taken to be $\Delta_{vir} = 101$ (Bullock et al. 2001). In equation (10) M_{vir} includes the baryonic mass, M_b ($M_{vir} = M_d + M_b$). Assuming a baryon fraction $f_b = \Omega_b/\Omega_M = 0.17$ (see next section), we have $M_{vir} \sim 1.2 \, M_d$ and equation (10) can be written explicitly for M_d as

$$c_d(M_d) \simeq 16.7 \left(\frac{M_d}{h^{-1} 10^{11} \text{ M}_\odot} \right)^{-0.125}. \tag{11}$$

Using this correlation, NFW profiles can thus be considered as a one-parameter density distribution (characterized by M_d or c_d).

The NFW profiles were produced in the framework of non-interacting (N-body) particles, but real galaxy formation includes baryons, whose interactions could modify the dark-matter mass profiles significantly – especially in their centres. Including these baryonic effects (cooling, star formation, heating, etc.) can be considered the 'holy grail' of galaxy formation theory, and there are currently efforts underway in this direction (Meza et al. 2003; Sommer-Larsen, Götz & Portinari 2003; Weinberg et al. 2004; Sáiz, Domínguez-Tenreiro & Serna 2004; Wright et al. 2003; Mo & Mao 2004). However, it seems that even the qualitative effects on the mass profiles are not yet known with any certainty, so we are simply taking the NFW profiles as the first approximation to the predictions of ΛCDM. Some possible implications of baryonic effects are discussed in Section 5.

3.3 The stellar mass fraction

From the previous sections, we see that early-type galaxy mass distributions in the ΛCDM framework can be approximated fairly well as a family of two parameters (for instance, M_d and M_*). We would further like to parametrize the stellar-to-dark mass ratio M_*/M_d. Although dark matter could be stripped from the halo, and baryons could be lost or gained through inflows and outflows, for want of more detailed knowledge we assume that the baryon fraction in the galaxy halo is the same as the universal value: $f_b = \Omega_b/\Omega_M$. This latter quantity is well constrained from the measurements of the cosmic microwave background, and here we adopt $f_b = 0.17$

---

[1] Navarro et al. (2004) provide a more detailed analysis of the density profiles (see also Mamon & Łokas 2004b), but using these profiles would change $M_{d,out}$ and $\nabla_\ell \Upsilon$ by only $\sim$10 per cent, which does not affect our conclusions in this paper.

[2] We have derived equation (10) in our assumed $\sigma_8 = 0.9$ cosmology in the halo mass range $M_{vir} = 0.03$–$30 \times 10^{12} \text{ M}_\odot \, h^{-1}$ via the toy model code provided by J. Bullock.
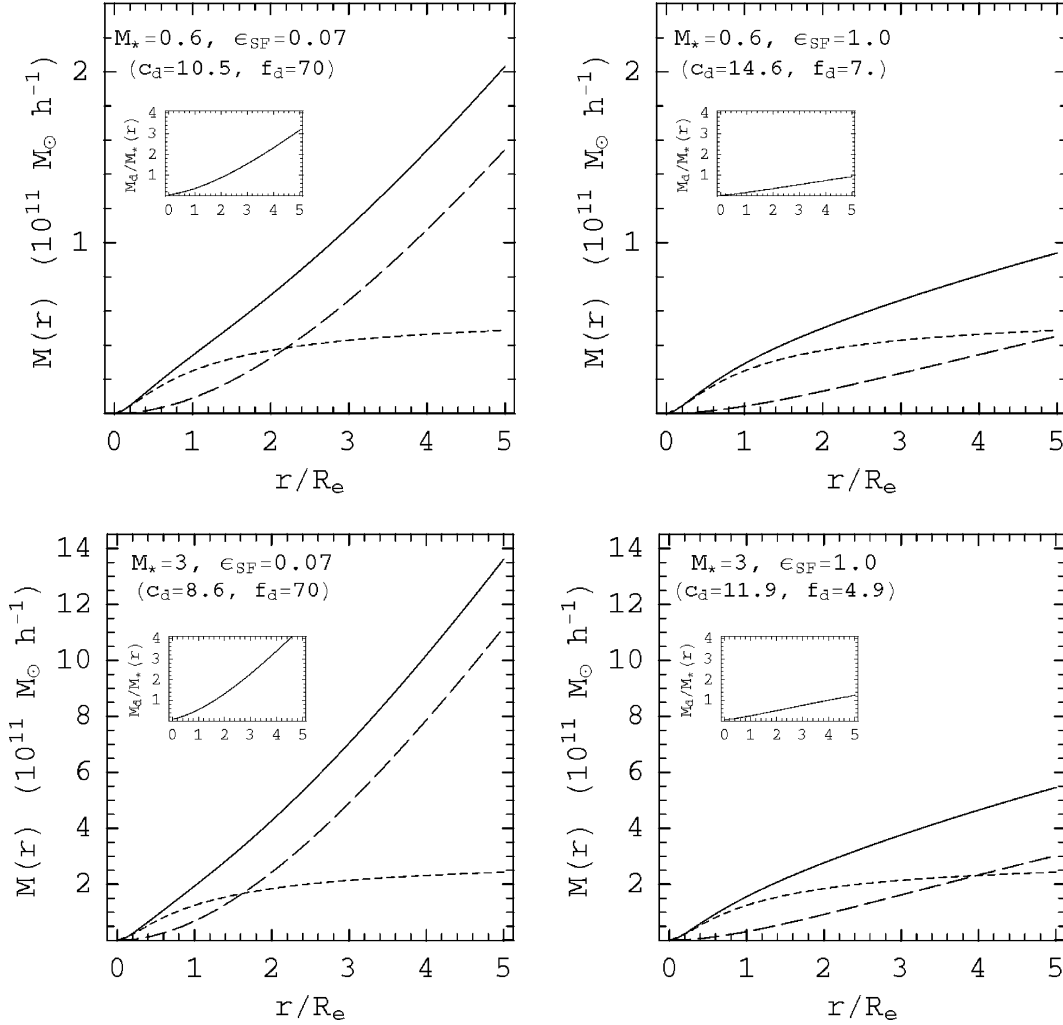
Figure 1. Profiles of enclosed mass with radius. Each panel shows a galaxy with parameters indicated. The solid curve is the total mass, and the dashed curves are the stellar and dark mass. Insets show the dark-to-luminous mass fraction as a function of the radius. These grow almost linearly outside $1R_e$. Within $0.5R_e$ the dark-matter fraction ranges between 10 and 20 per cent.

(Bennett et al. 2003). We relate this to the net star formation efficiency ϵ_{SF} (including stellar mass loss) by the following:

$$f_b^{-1} = \frac{M_{vir}}{M_b} = \frac{M_b + M_d}{M_b} = 1 + \frac{\epsilon_{SF} M_d}{M_*}, \qquad (12)$$

and thus $\epsilon_{SF} = 4.9 \, M_*/M_d$. While for physical insight, we will use ϵ_{SF} as our key parameter in this study, it should be remembered that this is a valid characteristic only if baryons are indeed conserved. Thus we will also quote the more robust dark-to-luminous mass fraction parameter $f_d \equiv M_d/M_* = 4.9/\epsilon_{SF}$.

There are no a priori constraints on ϵ_{SF}, although galaxy formation models use values in the range ~ 0.2–1.0 (Benson et al. 2000). Its extreme upper limit (given the baryon conservation assumption) is $\epsilon_{SF} = 1.0$ ($f_d = 4.9$), while its lowest limit can be taken from the universal average star formation efficiency of $\epsilon_{SF} = 0.072$ ($f_d = 68$; Fukugita, Hogan & Peebles 1998) and the assumption that early-type galaxies are at least as efficient as this, because clusters and groups bring the average down significantly. Studies matching mass and luminosity functions of virialized systems have suggested $\epsilon_{SF} \sim 0.25$ ($f_d \sim 20$) for typical galaxies (Marinoni & Hudson 2002; Guzik & Seljak 2002), while stellar masses in the SDSS survey (Padmanabhan et al. 2004) implied $M_{vir}/M_* = 7$–30 and $f_d \sim 6$–

25 ($\epsilon_{SF} \sim 0.2$–0.8). In the following we will consider conservatively $\epsilon_{SF} \sim 0.07$–1.0 as our lower and upper limits, respectively. We thus construct a sequence of ΛCDM-based galaxy models characterized by M_* and ϵ_{SF}. In real galaxies, the scatter in the R_e–M_* and c_d–M_d relations would produce considerable variation about this sequence, but for now we are considering the mean properties which should be apparent in a large enough sample of galaxies. In Fig. 1, we show some example mass profiles, where typical values for M_* are assumed, and extreme cases of $\epsilon_{SF} = (0.07, 1.0)$ are used. Note that in all cases, the dark matter is the dominant mass component by 5 R_e, indicating that early-type galaxies should generically show appreciable M/L gradients by this radius. The fraction of the total mass in dark matter within 0.5 R_e is in these cases 10–20 per cent (increasing with M_* and decreasing with ϵ_{SF}).[3] It is also evident in Fig. 1 that the M/L gradient is more strongly dependent on ϵ_{SF} than on M_*, which arises because R_e/r_s scales weakly with mass (and thus galaxies with a given f_d are a nearly homologous family). In

---

[3] Testing alternative parameter values in the R_e–M_* relation (equation 5) of $\alpha = 0.4$–1.2 does not change the conclusion that the dark-matter fraction at R_{in} is small.
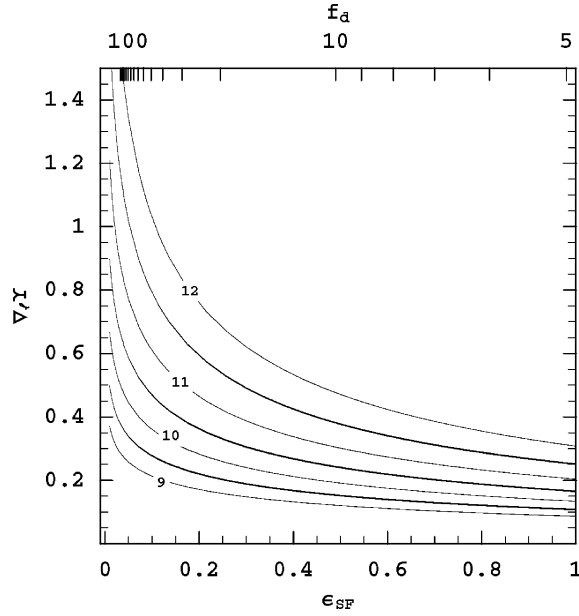
Figure 2. Predictions for the *M/L* gradient versus star formation efficiency. The curves are for stellar masses $\log(M_*/M_\odot)$ of 9.0–12.0 (marked in the plot), in increments of 0.5 (stellar luminosities M_B of -15.0 to -23.7, assuming $\Upsilon_* = 6.5$). The top axis shows the equivalent dark-to-luminous mass ratio $f_d = M_d/M_*$.

Figure 3. Predictions for the *M/L* gradient versus total stellar mass from ΛCDM, for different values of the star formation efficiency ϵ_{SF}. The solid curves show solutions with the nominal R_e–M_* relation of $(\alpha, R_M) = (0.56, 3.6)$; they are labelled at the right side by the values of ϵ_{SF} and the equivalent f_d (dark-to-luminous mass ratio). Heavy curves are physically plausible solutions, and light curves are not. Short-dashed lines show the prediction for the shallower R_e–M_* relation for dwarf galaxies $(\alpha, R_M) = (0.14, 1.57)$: this is only indicative as it is based on an $R^{1/4}$ light distribution, which is not appropriate for dwarf systems. Dot-dashed and long-dashed curves show the predictions assuming $(\alpha, R_M) = (0.4, 4.4)$ and $(1.2, 1.4)$, respectively; solutions are plotted for $\epsilon_{SF} = 0.07, 0.25, 1.0$.

the same figure, inset panels show $M_d(r)/M_*(r)$; this mass ratio does not significantly deviate from a linear growth curve at $r \gtrsim 0.5 \, R_e$, except for the case of very low ϵ_{SF} (i.e. very dark-matter-dominated haloes) and thus the measurement locations in equation (2) are generally not important (see also the next section).

3.4 *M/L* gradient predictions

We compute the model *M/L* gradients $\nabla_\ell \Upsilon$ (equation 2) with $r_{in} = 0.5 \, R_e$ and $r_{out} = 4 \, R_e$ representing typical values for the empirical measurements in Section 4.1. In Fig. 2, we plot the predicted $\nabla_\ell^{mod} \Upsilon$ versus ϵ_{SF} for sample galaxy models with various values of M_*. The gradient increases for decreasing ϵ_{SF}, as low-efficiency systems imply relatively more massive dark haloes. In Fig. 3, we plot the $\nabla_\ell^{mod} \Upsilon$ versus galaxy mass M_* for various values of ϵ_{SF}. The gradient increases with M_*, which can be qualitatively understood by the construction that the scaleradius of the stars varies more rapidly with mass ($R_e \propto M_*^{0.56}$) than the scaleradius of the dark matter ($r_s \propto r_{vir} c_d^{-1} \propto M_d^{0.33} M_d^{0.13} \propto M_d^{0.46}$). Thus the stellar body of a brighter galaxy encloses a larger fraction of its dark-matter halo than in a fainter galaxy, and appears more dark-matter dominated. This also means that in brighter galaxies, $\nabla_\ell \Upsilon$ is more sensitive to ϵ_{SF} than in fainter galaxies (see Fig. 2).

Although these predictions appear uniquely determined for given (ϵ_{SF}, M_*), there is an R_e–M_* scaling relation implicitly assumed (equation 5), which translates into assumed locations for (r_{in}, r_{out}). We therefore check the effects on the model predictions of the R_e–M_* relation. In Fig. 3 we show the predicted $\nabla_\ell \Upsilon$ – M_* curves for $(\alpha, R_M) = (0.4, 4.4)$ and $(1.2, 1.4)$, in addition to the nominal values of $(0.56, 3.6)$. The steep relation means a steeper trend for $\nabla_\ell \Upsilon$: for the more massive galaxies, R_e is larger for a given M_*, and thus the gradient probes farther into the dark-matter halo, producing higher values of $\nabla_\ell \Upsilon$. For the less massive galaxies, R_e is smaller, producing lower values of $\nabla_\ell \Upsilon$. With the shallow relation, r_s scales
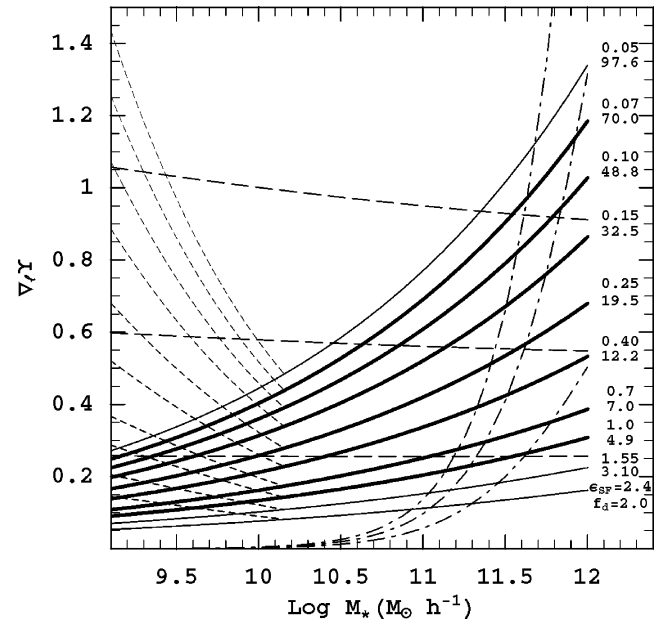
more quickly than R_e, and the $\nabla_\ell \Upsilon$ behaviour goes in the opposite direction, actually declining slightly with M_*.

Note that the mass of any diffuse gas [i.e. $M_g = M_* (1 - \epsilon_{SF})$] should add to the *M/L* gradient as a baryonic dark-matter component. However, assuming that this gas is distributed diffusely out to the virial radius (following the CDM density profile), its contribution to $\nabla_\ell \Upsilon$ is no more than ~ 0.02. We have also assumed that Υ_* is constant with radius, even if observed colour gradients of galaxies suggest a slight decrease with radius. Although it would be ideal to make our measurements in the K band rather than the B band in order to minimize this effect, we estimate the contribution to $\nabla_\ell \Upsilon$ in our current calculations to be only ~ -0.02. We also test the sensitivity of $\nabla_\ell \Upsilon$ to its measurement locations (r_{in}, r_{out}); these are important only for very dark-matter dominated systems, such that a value of $\nabla_\ell \Upsilon \sim 1.0$ changes by ~ 0.1 if $r_{out} \sim \pm 2 \, R_e$.

Our model galaxy constructions based on ΛCDM theory thus make specific predictions for *M/L* gradients. The quantity $\nabla_\ell \Upsilon$ increases with M_* unless ϵ_{SF} systematically increases with M_*, or the scaling parameter α is very high. If dEs do indeed follow a shallower scaling relation α, then $\nabla_\ell \Upsilon$ should increase again at low M_* (cf. Dekel & Silk 1986), with a minimum occurring at $\log M_*/(h^{-1} \, M_\odot) \sim 10.2$.

4 OBSERVATIONAL RESULTS

We describe our compilation of *M/L* results for early-type galaxies in Section 4.1. We study the R_e–M_* relation in Section 4.2, and

search for correlations between parameters in Section 4.3. Hereafter we assume $H_0 = 70$ km s^{-1} Mpc^{-1}.

4.1 Galaxy sample

We assemble from the literature the dynamical results on all early-type galaxies with mass measurements at a radius $r_{out} \gtrsim 2\,R_e$. These exclude galaxies with masses derived through X-ray analyses, SGL and gas discs and rings, as these techniques may be prone to strong selection effects. For instance, X-ray emission occurs mostly in giant elliptical galaxies, so these results are restricted to the brightest, most massive systems – mostly group or cluster dominant ellipticals (see O'Sullivan & Ponman 2004b for a discussion). Gravitational lensing also suffers a selection effect for large masses, as the lensing cross-section is a power law of the lens mass. Furthermore, the systems studied by lensing are generally located at large redshifts $0.1 < z < 1$ (Treu & Koopmans 2004): here it appears that low-mass galaxies are still forming stars while only very massive galaxies are already in place (Jimenez et al. 2005). This makes the selection effect even worse if we want to compare results with local galaxies. Extended H I rings (which are rare occurrences) are mostly located in S0 systems. Furthermore, in most of the cases, these systems are gas rich ($M_{HI}/L_{B,\odot} \gtrsim 0.2$) which suggests that these galaxies are the result of a particular formation history (merging remnants of gas-rich discs, Oosterloo et al. 2002) and are not representative of the ellipticals on the whole. Thus, none of these methods is really suitable for an unbiased survey of the properties of dark-matter haloes around elliptical galaxies.

The techniques remaining include integrated stellar light, PNe and GCs; there is no obvious reason for any of these to produce a particular selection effect on total mass (rather than on luminosity). The results could in principle be skewed by dust effects when relying on integrated stellar light kinematics (Baes & Dejonghe 2001), but the halo masses of most of the sample galaxies are derived from discrete tracers (PNe and GCs), which are not affected by this issue. There are 21 galaxies in the sample (16 ellipticals, three lenticulars and two of a transitional nature); their properties are summarized in Table 1, including a_4 (isophote shape parameter) and γ (inner surface brightness slope). Note that this sample includes two cD galaxies, whose halo masses may very well be dominated by the galaxy cluster in which they reside. However, this may also be true of group-dominant galaxies in general, and at this point we do not wish to make such a priori distinctions; we will check any density environment dependence later on.

Some of the dynamical M/L values (Υ_{in}, Υ_{out} – provided in the B band for uniformity) are derived from highly flexible modelling techniques which fit orbital distributions to the detailed line-of-sight velocity distributions (Kronawitter et al. 2000; Gebhardt et al. 2003; Romanowsky et al. 2003). For these we take the uncertainties in Υ as given in the papers. In other cases, Jeans (and similar) models have been used to fit binned velocity dispersion profiles; in such models, orbital anisotropy is a major source of systematic uncertainty. Although not many detailed dynamical studies have extended beyond $2\,R_e$, so far no cases of extreme anisotropy have been detected (see e.g. Gerhard et al. 2001). We therefore assume that the anisotropy parameter β_a lies in the range ± 0.3 ($\beta_a = 0$ is isotropic), and estimate uncertainties in Υ_{in} of ± 10 per cent and in Υ_{out} of ± 30 per cent.

To find the empirical gradient $\nabla_\ell^{obs}\Upsilon$, we also need to know Υ_*, which may be estimated in two completely independent ways. We can use spectroscopic information for the luminous body combined with (single-burst) stellar population synthesis models: $\Upsilon_* = \Upsilon_{SSP}$.

This is in principle the most direct way to measure the stellar mass only, but currently such models are susceptible to considerable systematic uncertainties. The second way is to use the dynamical estimate: $\Upsilon_* = \Upsilon_{in}$; there will be some dark-matter contribution to Υ_{in}, so this approach will provide a lower limit on $\nabla_\ell^{obs}\Upsilon$. The advantage of this approach is that many systematic uncertainties (such as distance) will cancel out in equation (2); the empirical gradient is thus

$$\nabla_\ell^{obs}\Upsilon = \frac{R_e}{r}\left(\frac{\Upsilon_{out}}{\Upsilon_{in}} - 1\right) . \tag{13}$$

We first check the reliability of these two approaches by comparing their results in a common galaxy subsample. The mean stellar age and metallicity are taken from Terlevich & Forbes (2002), or if unavailable, from Trager et al. (2000) or from Kuntschner et al. (2001); note $r_{in} = R_e/8$ generally. We then obtain the expected B-band stellar M/L, Υ_{SSP}, using stellar population synthesis models from Worthey (1994). After examining galaxies in common in order to tie the results on to a uniform scale, we increase the Υ_{SSP} values from Trager et al. (2000) by 15 per cent and decrease those from Kuntschner et al. (2001) by 8 per cent. The results for the 15 galaxies with available age and metallicity are listed in Table 1. We compare Υ_{SSP} to the innermost dynamical estimates Υ_{in} in Fig. 4, and find them to be remarkably consistent given all the potential sources of error which have not been included in the uncertainties (e.g. distance, IMF, heterogeneous r_{in}/R_e). This consistency indicates that if some fraction of Υ_{in} comes from dark matter, then Υ_{SSP} has been systematically overestimated by approximately the same amount. We will thus assume $\Upsilon_* = \Upsilon_{in}$ for all our ensuing analyses, also examining in due course the potential effects of a non-negligible dark-matter contribution.

A best fit of Υ_* to galaxy luminosity and mass shows a weak correlation: $\Upsilon_{B,*} \propto L_B^{0.07\pm0.06}$; $\Upsilon_{B,*} \propto M_*^{0.10\pm0.06}$. This is weaker than some of the trends found in the literature (see Section 3.1), but Kauffmann et al. (2003) and Padmanabhan et al. (2004) also find Υ_* to be roughly constant. The models of the latter two imply $\Upsilon_* \sim 5$ in the B band, while we obtain ~ 7 typically, lending credence to the possibility that we are underestimating the amount of dark matter in the central parts of our galaxy sample.

4.2 Mass–radius relation

As seen in Section 2, to derive the M/L gradient predictions, we needed a mean relation between R_e and M_* (equation 5), where we adopted values for the parameters (α, R_M) based on literature results. For direct comparison to our empirical M/L gradient results, we must check that our galaxy sample is consistent with this relation. We begin by fitting a mean R_e–M_* relation to our sample (as shown in Fig. 5), where M_* is obtained by multiplying Υ_* and the total luminosity L_B. We find (α, R_M) = (0.50 $\pm$ 0.13, 3.6 $\pm$ 0.8), which is consistent with (0.56, 4.2; $h = 0.7$) from Shen et al. (2003). As this fit is sensitive to sparse sampling effects in our data set, we instead wish to use an exponent α based on the much larger SDSS galaxy sample, with the normalization R_M set by our data owing to systematic differences in measuring masses and sizes. Assuming a typical $\alpha = 0.6$ (see Section 3.1), we find $R_M = 3.1 \pm 0.8$; for comparison $R_M = 4.2$ from Shen et al. (2003),[4] and the Pahre et al. (1998) results (where also $\alpha \sim 0.6$) imply

---

[4] This is consistent with their Υ_* values (obtained via population synthesis modelling; Kauffmann et al. 2003) being systematically lower than ours.

Table 1. Catalogue of early-type galaxies with halo mass measurements.

Galaxy	Type[a]	D^b (Mpc)	M_B	R_e^c (kpc)	a_4^d	γ	r_{in} (R_e)	Υ_{in} $(\Upsilon_{B,\odot})$	r_{out} (R_e)	Υ_{out} $(\Upsilon_{B,\odot})$	Υ_{SSP} $(\Upsilon_{B,\odot})$	$\nabla_\ell\Upsilon$	Data type;[e] $\Upsilon_{in,out}$ Ref.[g]
NGC 221	E3	0.9	−16.5	0.2	0.0	0.5	0.1	2.8 ± 0.2	5.6	4.8 ± 2.8	$3.0^{+0.9}_{-0.7}$	0.13 ± 0.18	LS, PNe; MB01, V02
NGC 821	E2	25.5	−20.6	6.2	2.5	0.64	0.5	8.4 ± 0.4	4.8	13.1 ± 3.9	$7.1^{+1.9}_{-2.0}$	0.13 ± 0.10	LS+PNe; G03, R03
NGC 1316	S0	22.7	−22.1	12.0	0.0	0.0	0.6	3.2 ± 0.3	2.	5.7 ± 1.7	$3.9^{+0.8}_{-1.1}$	0.56 ± 0.39	LS+PNe; A98
NGC 1379	E0	21.2	−19.8	2.5	0.2	-	0.4	4.4 ± 0.4	2.5	4.4 ± 0.4	$7.4^{+2.5}_{-2.0}$	0.0 ± 0.07	LS; MB01
NGC 1399[f]	E1/cD	21.1	−21.4	4.3	0.1	0.07	1.0	8.3 ± 0.8	12.0	42.0 ± 13.0	$10.4^{+3.3}_{-2.7}$	0.37 ± 0.14	LS+GCs; S00, R04
NGC 1700	E4	52.0	−21.7	3.5	0.4	0.01	0.5	4.0 ± 0.4	4.6	7.8 ± 0.8	3.3 ± 0.4	0.23 ± 0.06	LS; S99
NGC 2434	E1	22.8	−20.5	2.7	0.0	0.7	0.5	8.2 ± 0.3	2.6	15.8 ± 3.4	–	0.44 ± 0.20	LS; K00
NGC 3115	E6/S0	10.2	−20.2	2.8	1.0	0.78	0.8	6.0 ± 0.6	3.3	10.0 ± 2.0	–	0.27 ± 0.14	LS; C93, E99
NGC 3379	E1	11.2	−20.1	2.0	0.2	0.18	0.5	5.9 ± 0.4	7.9	8.7 ± 1.1	$8.4^{+2.8}_{-2.4}$	0.06 ± 0.03	LS+PNe; G03, R03
NGC 3384	E5/S0	12.3	−19.8	1.5	1.0	0.6	0.5	4.1 ± 0.4	5.8	7.4 ± 2.2	3.2 ± 0.6	0.15 ± 0.1	LS, PNe; T95, B96
NGC 4406	E3	18.1	−21.6	8.9	−0.7	0.08	0.3	6.4 ± 0.7	2.4	11.4 ± 3.4	$8.1^{+2.4}_{-2.2}$	0.37 ± 0.23	LS, PNe; M91, A96
NGC 4464	S0/a	15.3	−18.7	0.45	0.5	0.88	0.5	7.9 ± 0.8	2.8	8.7 ± 2.6	$4.6^{+1.7}_{-0.7}$	0.04 ± 0.15	LS; MB01
NGC 4472	E2	17.2	−22.	8.7	−0.3	0.04	0.5	8.0 ± 0.3	4.5	28.5 ± 8.6	$8.4^{+2.2}_{-2.3}$	0.64 ± 0.27	LS, GCs; K00, C03
NGC 4486	E3/cD	17.0	−21.7	7.8	0.0	0.2	0.5	5.3 ± 0.4	4.8	30.0 ± 4.5	–	1.1 ± 0.2	LS+GCs; RK01
NGC 4486B	E1	17.0	−16.8	0.26	0.8	0.14	0.2	8.1 ± 0.6	2.8	10.3 ± 2.2	–	0.1 ± 0.11	LS; K00
NGC 4494	E1	18.0	−20.7	4.3	0.3	0.6	0.5	3.9 ± 0.4	3.9	5.5 ± 1.7	–	0.12 ± 0.13	LS, PNe; K00, R03
NGC 4697	E3	12.4	−20.2	5.7	1.4	0.74	0.4	9.3 ± 0.4	3.4	9.3 ± 2.8	$6.7^{+2.3}_{-1.7}$	0.0 ± 0.1	LS, PNe; M01
NGC 5128	S0	4.4	−21.	6.6	−0.5	0.15	0.3	2.8 ± 0.3	10	10.0 ± 3.0	–	0.27 ± 0.07	PNe; P04
NGC 5846	E1	26.3	−20.4	8.0	0.0	<0.2	0.5	9.0 ± 1.0	3.2	20.0 ± 6.0	$11.1^{+3.7}_{-3.2}$	0.45 ± 0.25	LS; MB01
NGC 6703	E1	28.2	−20.3	4.1	0.0	-	0.5	5.3 ± 0.3	2.6	7.6 ± 2.3	4.7 ± 1.0	0.21 ± 0.21	LS; K00
NGC 7626	E2	46.0	−21.4	8.5	0.2	<0.2	0.5	10.0 ± 0.6	2.1	18.3 ± 3.6	$10.8^{+3.6}_{-3.1}$	0.52 ± 0.23	LS; K00

Notes. [a]Types and magnitudes from HyperLeda (http://www-obs.univ-lyon1.fr/hypercat/). [b]Distances from SBF measurements (Tonry et al. 2001), rescaled from $h = 0.74$ to $h = 0.70$. The exceptions are NGC 4486B (which is assigned the same distance as NGC 4486) and NGC 1700, 4464 and 7626, for which the redshift distance is used. The distance uncertainties are taken from the SBF paper and included in any uncertainties in M_B and M_*, but are not included in the Υ uncertainties shown here because they cancel out when calculating $\nabla_\ell\Upsilon$. [c]For consistency, R_e is taken from the dynamical reference paper. [d] a_4 and γ are taken from Bender, Burstein & Faber (1992), Forbes, Franx & Illingworth (1995), Faber et al. (1997), Pellegrini (1999), Trager et al. (2000), Ravindranath et al. (2001); and references therein. [e]LS = long-slit integrated light stellar kinematics; PNe = planetary nebulae; GCs = globular clusters. [f]The PNe and GC results from Napolitano et al. (2002) ($M/L \sim 28$–45 at 8.8 R_e) imply $\nabla_\ell\Upsilon \sim 0.3$–0.58 depending on assumptions about the halo equilibrium. We use the R04 result when computing correlations. [g]References: MB01, Magorrian & Ballantyne (2001); V02, Verolme et al. (2002); R03, Romanowsky et al. (2003); A98, Arnaboldi et al. (1996); S00, Saglia et al. (2000); R04, Richtler et al. (2004); S99, Statler et al. (1999); K00, Kronawitter et al. (2000); C93, Capaccioli et al. (1993); E99, Emsellem et al. (1999); G03, Gebhardt et al. (2003); T95, Tremblay et al. (1995); B96, Busarello et al. (1996); M91, van der Marel (1991); A96, Arnaboldi et al. (1996); C03, Côté et al. (2003); RK01, Romanowsky & Kochanek (2001); M01, Méndez et al. (2001); P04, Peng et al. (2004).

$R_M = 2.6$ if $(B - K) = 4.1$ and $\Upsilon_* = 7$. Thus, our R_e–M_* relation is intermediate between typical literature values.

The uncertainties in this relation are important to consider when making predictions for $\nabla_\ell\Upsilon$. In particular, the exponent α is not yet known conclusively and may systematically vary with M_*; we have seen in Section 3.4 how changes in α would affect the model predictions for $\nabla_\ell\Upsilon$. We have also seen that, even if α is

known accurately, there is a large scatter in real galaxies around the mean R_e–M_* relation (which is after all only a projection of the FP). So when we later come to M/L results in Fig. 7, these should not be overinterpreted for any single galaxy; rather, the mean trends in a large sample of galaxies are meaningful. We can quantify the effects of the scatter by finding an 'envelope' for the R_e–M_* relation, enclosing 68 per cent of the data

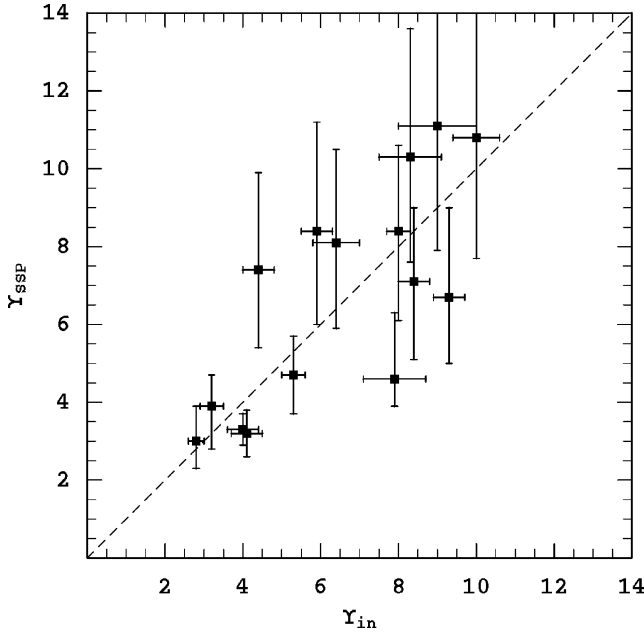**Figure 4.** Estimates of stellar M/L from stellar population synthesis modelling (Υ_{SSP}) compared to dynamical modelling (Υ_{in}), in units of $\Upsilon_{B,\odot}$. The dashed line shows $\Upsilon_{in} = \Upsilon_{SSP}$.
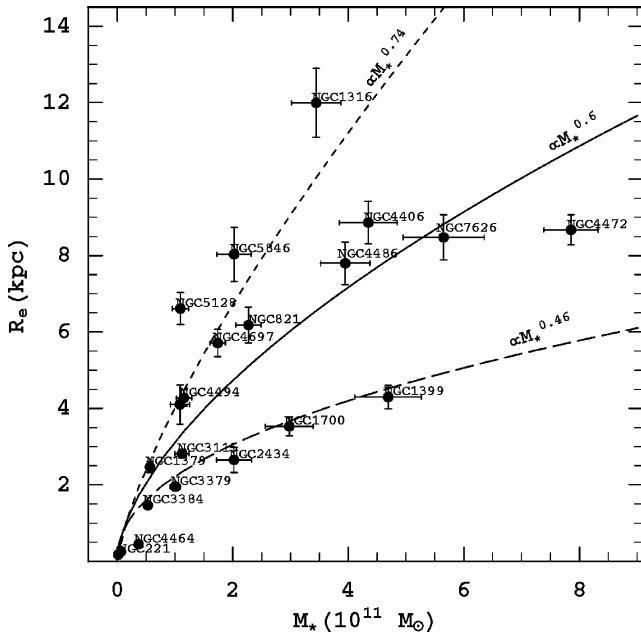

Figure 5. Relation between total luminous mass and effective radius. The solid line is the best fit to the data ($\alpha = 0.6$, $R_M = 3.2$) and the dotted and dashed lines show the $\pm 1\sigma$ uncertainties of the fit: ($\alpha = 0.74$, $R_M = 4.0$) and ($\alpha = 0.46$, $R_M = 2.4$), respectively.

points. The upper and lower envelopes have (α, R_M) = (0.74, 4.0) and (0.46, 2.4), respectively (see Fig. 5); these values are well within the plausible bounds on α of 0.4–1.2 discussed in Section 3.1. Thus when we compare to theoretical models in Section 5, we can safely use ($\alpha = 0.6$, $R_M = 3.1$), based on larger galaxy surveys, as representative of our sample; and we can check the effects of allowing (α, R_M) to vary within plausible limits.

4.3 Correlations

Before comparing the empirical results on the M/L gradient to theoretical predictions, we would like to see if there are any correlations in the data (see earlier work in Capaccioli, Napolitano & Arnaboldi 2003; Napolitano et al. 2004). The broadest property to test against is the total galaxy magnitude M_B. Plotting $\nabla_\ell^{obs}\Upsilon$ against M_B in Fig. 6, we see that fainter galaxies have shallow gradients ($\nabla_\ell^{obs}\Upsilon \sim 0.0$–0.1 for $M_B \lesssim -20$) while the brighter galaxies have a wide range of gradients ($\nabla_\ell^{obs}\Upsilon \sim 0.1$–0.6). The same trend is found when considering galaxy mass M_* (as estimated using $\Upsilon_* = \Upsilon_{in}$) rather than galaxy luminosity, with $\log M_* \sim 11.2$ marking the transition between shallow and steep gradients. We also see evidence in Fig. 6 for discy galaxies ($a_4 \gtrsim 0.2$) having shallow gradients while box-like ones have a wide range, and for galaxies with a steep central cusp ($\gamma \gtrsim 0.2$) having shallower gradients than those with a shallow cusp.

These last two trends are not surprising given the first, as it is well-established that galaxy properties such as a_4 and γ correlate strongly with luminosity (Nieto & Bender 1989; Capaccioli, Caon & D'Onofrio 1992; Faber et al. 1997). The strengths of the correlations as measured by the Spearman rank statistic r_{spear} (Press et al. 1992) are given in Table 2, where N is the number of galaxies. To estimate the statistical significance of these correlations, we performed, for each structural parameter, 10 000 random experiments where $\nabla_\ell\Upsilon$ have been randomly extracted for each galaxy according to a Gaussian measurement distribution. The confidence level of the correlations being real is then given in the table.

The correlations apparent by eye are all significant at the more than 97 per cent level, and the ones with M_B and M_* are the strongest. Note that these correlation results are independent of any distance uncertainties (which cancel out in the method used for estimating $\nabla_\ell^{obs}\Upsilon$). Nor are they changed if Υ_* is systematically wrong in the sense that there is a large, constant fraction of dark matter in the galaxy centres: this would change $\nabla_\ell^{obs}\Upsilon$ equally for all galaxies and would not affect their ordering. A possible effect is if $\Upsilon_* = \Upsilon_{in}$ is wrong by an amount, which varies systematically with M_B.

However, in our basic ΛCDM picture, Υ_* is likely to be systematically too *high* for the brightest galaxies (see Section 3.3), leading to $\nabla_\ell^{obs}\Upsilon$ estimates which are too *low*; thus, the 'corrected' values of $\nabla_\ell^{obs}\Upsilon$ would result in an even stronger correlation. Even if Υ_* were wrong in the opposite sense (such that Υ_*/Υ_{in} is actually much lower for low-L ellipticals), we estimate that dark-matter mass fractions of $\sim$50 per cent would be needed to explain the correlation – much larger than the fractions typically estimated from other studies.

As a final source of systematic effects in the M/L trends, we have checked any dependence of $\nabla_\ell^{obs}\Upsilon$ with the (density) environment. We used for this purpose the galaxy density estimates ρ_{env} (number of galaxies per Mpc^3) from Tully (1988) and compared with our $\nabla_\ell^{obs}\Upsilon$. We did not find any significant correlation with M/L gradients: the Spearman rank statistics gives a 78 per cent significance for a positive correlation. The steepest gradients (NGC 4486 and 4472) are indeed the ones related to the densest environment (but note that their close companions NGC 4486B and 4464 have low gradients). These are the only apparent cases where the environmental effect could have enhanced the gradients because of a cluster dark-matter background or the effect of a close encounter (see Napolitano et al. 2002 for NGC 1399).

We therefore conclude that there is a empirical trend for bright, boxy shallow-core early-type galaxies to appear more dark-matter dominated than faint, discy steep-core galaxies. This
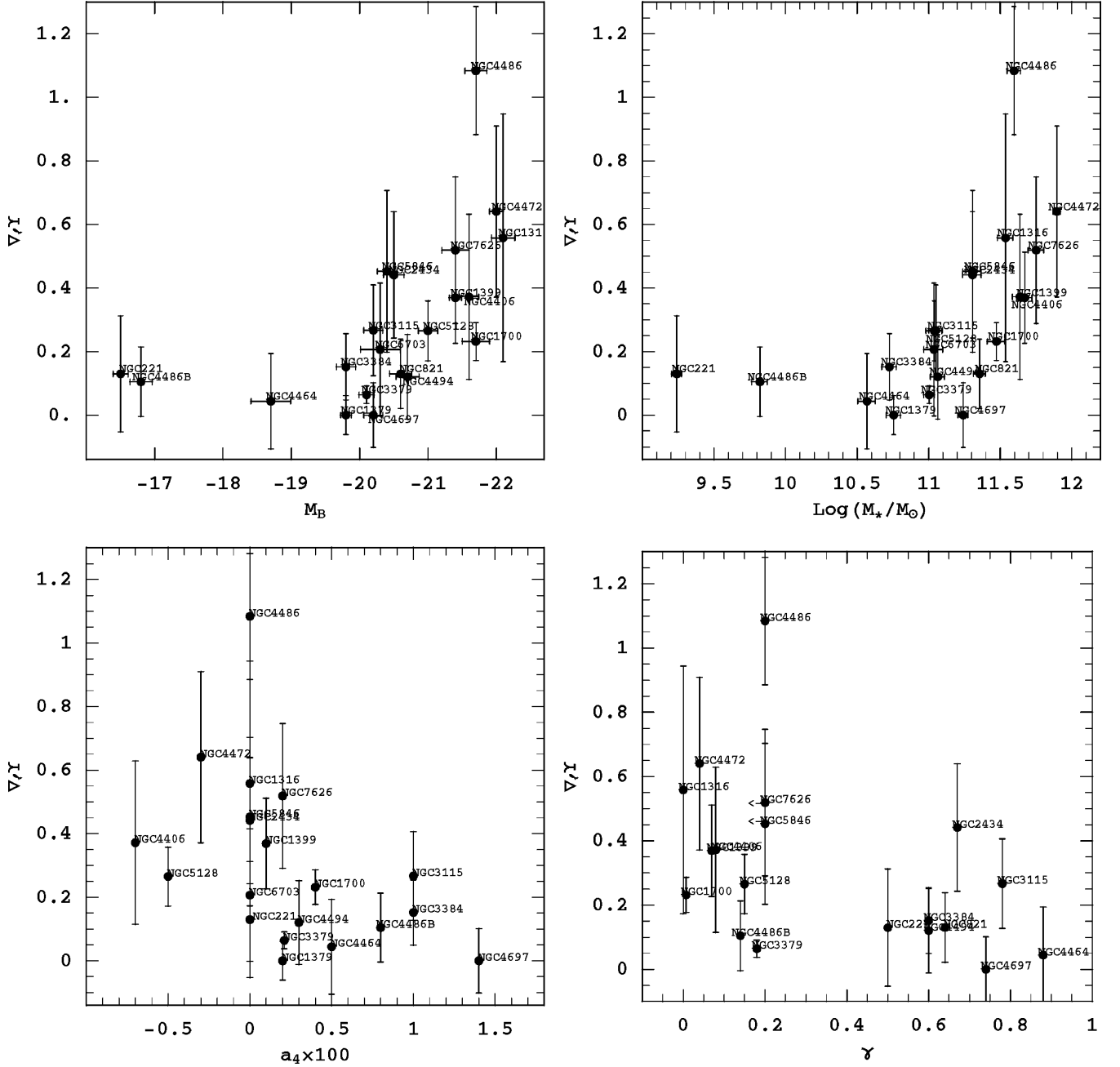
Figure 6. Empirical M/L gradients versus galaxy parameters: the total luminosity M_B (upper left), the total stellar mass M_* (upper right), the isophotal shape a_4 (lower left) and the central surface brightness slope γ (lower right). Error bars are 1σ level.

result is irrespective of the type of underlying dark-matter distribution and environment, but is especially strong if it resides in basic ΛCDM haloes.

5 IMPLICATIONS OF PREDICTIONS VERSUS OBSERVATIONS

In Section 5.1, we show the results on halo masses and implied ϵ_{SF} using the $\nabla_\ell^{obs}\Upsilon$ data from Section 4 in conjunction with the model predictions of Section 3.4. Finding many of the halo masses to be problematically low in the context of ΛCDM, we consider possible alternative explanations in Section 5.2. In Section 5.3 we briefly discuss the results based on other observation techniques

(X-rays, gravitational lensing and H I rings) and we lastly give some indication of the ϵ_{SF} inferred in a few systems from the very low-mass regime in Section 5.4.

5.1 Matching models and observations

We now compare the galaxy M/L gradient data, $\nabla_\ell^{obs}\Upsilon$, to the expectations from ΛCDM, and illustrate this in Fig. 7, where $\nabla_\ell^{mod}\Upsilon$ is plotted versus M_* for various values of ϵ_{SF} and using the best-fitting R_e–M_* relation ($\alpha = 0.6$, $R_M = 3.1$) together with the 68 per cent envelopes. We can see immediately that the data do not seem to follow the simple increase of $\nabla_\ell\Upsilon$ with M_* that is expected for a 'universal' ϵ_{SF}, and the empirical increase appears to be sharper.

Table 2. Spearman correlation test.

Correlation	N	r_{spear}	Confidence level
$\nabla_\ell \Upsilon - M_B$	21	-0.58	99.9 per cent
$\nabla_\ell \Upsilon - a_4$	21	-0.42	98 per cent
$\nabla_\ell \Upsilon - \gamma$	19	-0.39	97 per cent
$\nabla_\ell \Upsilon - M_*$	21	0.58	99.9 per cent
$\nabla_\ell \Upsilon - \rho_{\mathrm{env}}$	18	0.10	78 per cent
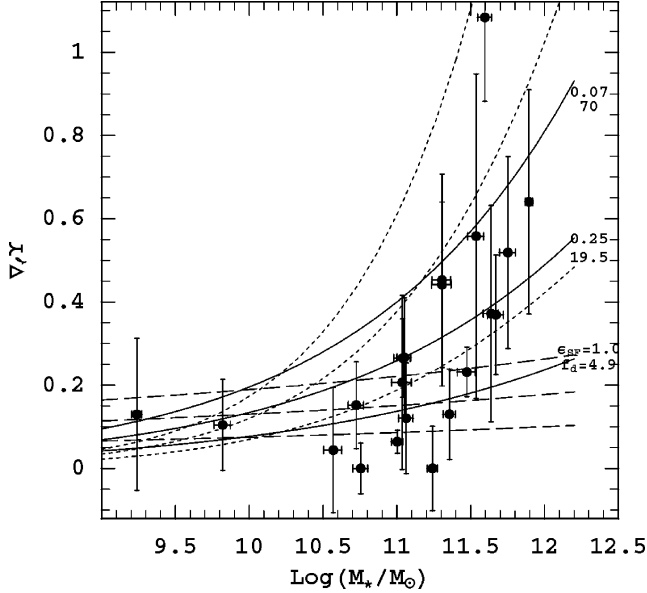
Figure 7. M/L gradients versus total luminous mass. Points with error bars show galaxy data with uncertainties. Labelled curves are our predictions from ΛCDM for different values of ϵ_{SF} and f_{d}: solid curves are models for the best-fitting $R_{\mathrm{e}}-M_*$ relation ($\alpha = 0.6$, $R_{\mathrm{M}} = 3.6$), short dashed and long-dashed curves are models for the 68 per cent envelopes as in Fig. 5.

By inspection of the figure, one interpretation is that the low-mass galaxies have very high values for ϵ_{SF} (in some cases even above the highest allowed limit) while the high-mass galaxies have a broad scatter in ϵ_{SF}, mostly within the allowed efficiency range. Note that projection effects in the dynamical modelling of Υ can produce systematic effects on the inferred $\nabla_\ell^{\mathrm{obs}}\Upsilon$: face-on discy galaxies could appear to have very low Υ_{out} if interpreted as spherical systems. This would produce some data points with spuriously low $\nabla_\ell^{\mathrm{obs}}\Upsilon$ (and high ϵ_{SF}) values, but these should comprise a small fraction of a large, unbiased sample.

To quantify the $\epsilon_{\mathrm{SF}} - M_*$ trend requires allowing for the departure of the individual galaxies from the mean $R_{\mathrm{e}}-M_*$ relation. To this end, we fit the model simultaneously to R_{e} and to $\nabla_\ell^{\mathrm{obs}}\Upsilon$ with free parameters $(\alpha, R_M, \epsilon_{\mathrm{SF}})$, minimizing the following χ^2 statistic:

$$\chi^2 = \sum_{i=1}^{2} \left(\frac{q_i - F_i}{\delta q_i} \right)^2, \tag{14}$$

where $q_1 = R_{\mathrm{e}}^{\mathrm{obs}}$, $F_1 = R_{\mathrm{M}}(M_*)^\alpha$, $q_2 = \nabla_\ell^{\mathrm{obs}}\Upsilon$, $F_2 = \nabla_\ell^{\mathrm{mod}}\Upsilon(\alpha, R_{\mathrm{M}}, \epsilon_{\mathrm{SF}})$ and δq_i are the uncertainties on q_i. The results are shown in Fig. 8 where we plot the best-fitting ϵ_{SF} (and equivalently f_{d}) against the stellar masses. From the distribution of the fitted values we have inferred the following median values: $\epsilon_{\mathrm{SF}} \sim 2.0^{+4.0}_{-0.8}$ for $\log M_* = 11.0^{+0.2}_{-0.4}$ and $\epsilon_{\mathrm{SF}} \sim 0.23^{+0.17}_{-0.13}$ for $\log M_* = 11.4^{+0.3}_{-0.2}$ (with a marginal overlap of the mass ranges around $\log M_* \sim 11.2$). There
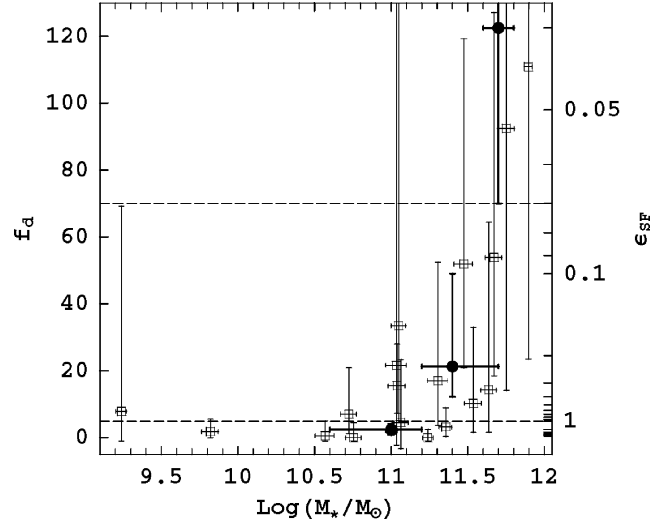
Figure 8. Efficiency of star formation versus total luminous mass, for early-type galaxy data fitted to ΛCDM models (open squares). Plausible upper and lower bounds on these parameters are shown as dotted lines. Full points are the median values from the distribution of the best-fitting values. The data points of NGC 2434 and 4486 are above the plot limits.

are also galaxies with $\log M_* = 11.7^{+0.1}_{-0.1}$ for which $\epsilon_{\mathrm{SF}} \sim 0.04^{+0.03}_{-0.04}$, only marginally consistent with the plausible lowest efficiency limit. These values suggest a smooth relation between M_* and ϵ_{SF} (see Fig. 8) which is at this stage only tentative because of the large uncertainties in the data.

An alternative interpretation is the presence of a mass scale $[\log(M_0/\mathrm{M}_\odot) \sim 11.2, M_0 \sim 1.6 \times 10^{11}\,\mathrm{M}_\odot]$ marking a clear dichotomy: galaxies with $M_* \gtrsim M_0$ are most consistent with $\epsilon_{\mathrm{SF}} \sim 0.25$ ($f_{\mathrm{d}} \sim 19.5$), while galaxies with $M_* \lesssim M_0$ are most consistent with $\epsilon_{\mathrm{SF}} \sim 2$ ($f_{\mathrm{d}} \sim 3$). In the latter sample, half of these are well determined to have $\epsilon_{\mathrm{SF}} > 0.9$ ($f_{\mathrm{d}} < 5.4$), while those galaxies with lower ϵ_{SF} (larger $\nabla_\ell^{\mathrm{obs}}\Upsilon$ in Fig. 7) are boxy systems, in agreement with the tentative dichotomy discussed at the end of Section 4.3. This suggests that there are separate populations of galaxies with very different ϵ_{SF}, rather than a trend of ϵ_{SF} with M_* for a single galaxy population – but we cannot distinguish between these two scenarios given the large uncertainties in the current data.

Note that other studies have suggested a maximum galaxy formation efficiency (minimum dark-to-luminous mass fraction, f_{d}) at M_* close to our M_0 (Benson et al. 2000; Marinoni & Hudson 2002; Romano et al. 2002). Assuming an average $\Upsilon_* = 6.5$, as in our sample, we can convert this mass scale into a luminosity scale of $M_B = -20.5$, fairly similar to the luminosity scale found in other luminous properties of early-type galaxies (Graham et al. 2003; Graham & Guzmán 2003).

The $\epsilon_{\mathrm{SF}} \sim 0.25$ value for the high-mass galaxies is logarithmically midway between the uppermost and lowermost limits adopted. However, $\epsilon_{\mathrm{SF}} \sim 2$ is unphysical for the low-mass galaxies, given the assumptions of our ΛCDM models. To understand the origin of these ϵ_{SF} values in the ΛCDM models, in Fig. 9 we plot $\nabla_\ell^{\mathrm{mod}}\Upsilon$ again as a function of M_* with curves of constant c_{d} now indicated. At each point on the curve, ϵ_{SF} has been adjusted to fit the required ΛCDM $c_{\mathrm{d}} - M_{\mathrm{d}}$ relation. For a low stellar mass galaxy ($M_* < M_0$) to have a shallow M/L gradient, its ΛCDM concentration must be high ($c_{\mathrm{d}} \gtrsim 15$), which implies a small halo mass. This mass corresponds to $\epsilon_{\mathrm{SF}} > 1$ and thus to a violation of baryon conservation. To show this, we plot in Fig. 10 the baryon fraction f_{b} as a function of c_{d},
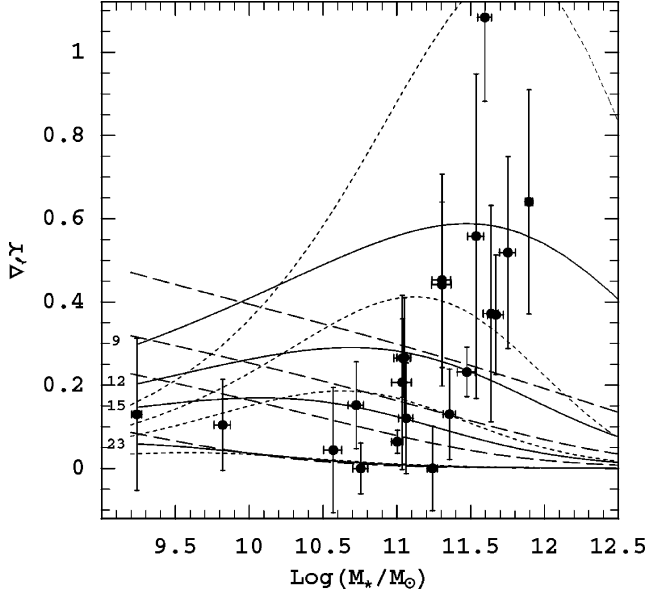
Figure 9. M/L gradients versus total luminous mass, with curves shown of constant concentration parameter c_d, according to the ΛCDM predictions, with ϵ_{SF} free to vary. Line styles are as in Fig. 7.
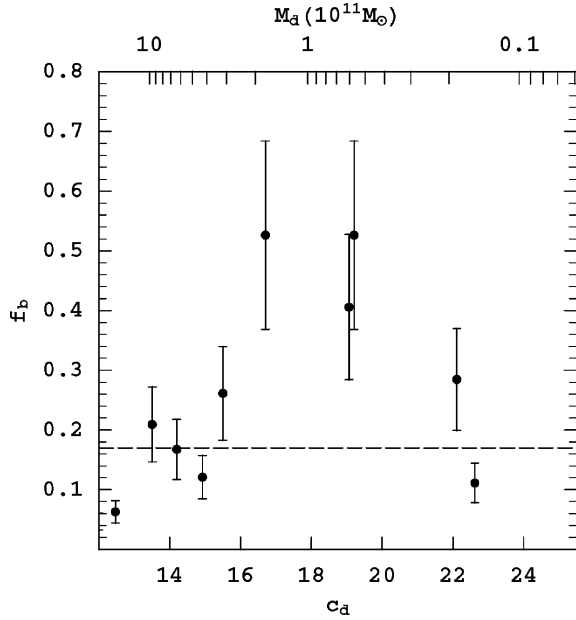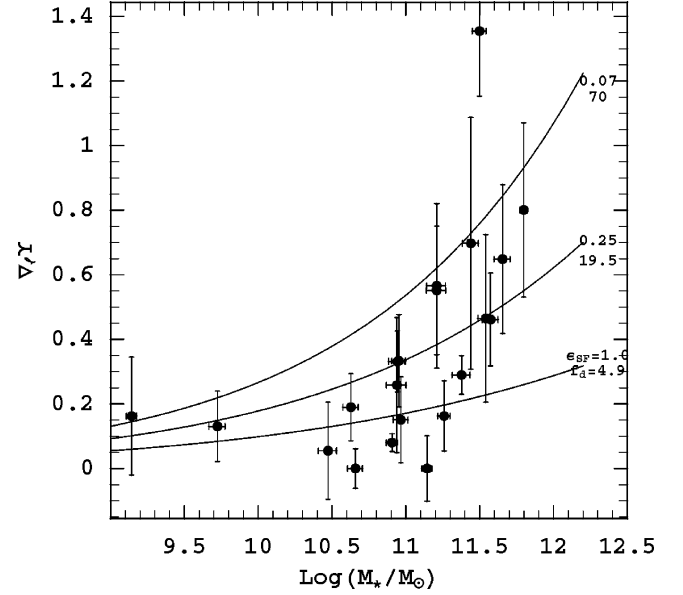

Figure 11. M/L gradients versus total luminous mass accounting for 30 per cent dark mass in the inner regions. Line styles have the same meaning as in Fig. 7. The position of the data points relative to the model curves is almost unchanged with respect to Fig. 7.

Figure 10. Baryon fraction for the low-mass systems ($M_* < M_0$) as a function of the halo concentration c_d: here the high $c_d \gtrsim 13$ range is shown. Halo masses are inferred by their best-fitting c_d according to the c_d–M_d and shown on the upper axis. Dashed line marks the cosmological baryon fraction, $f_b = 0.17$.

where the f_d results (Fig. 8) have been re-interpreted with the assumption $\epsilon_{SF} = 1.0$, giving $f_b = 1/(1 + 1.0 f_d)$. We find that many of the galaxies with $c_d \gtrsim 15$ have $f_b \gg 0.17$, a circumstance which gets worse if $\epsilon_{SF} < 1$.

5.2 Discussion

In the previous section we have seen that the basic assumption of ΛCDM (namely the c_d–M_d relation) and baryon conservation with

$f_b = 0.17$ lead to typical formation efficiencies $\epsilon_{SF} \sim 0.25$ for galaxies with $M_* > M_0$, while in the low-mass regime ($M_* < M_0$) they produce unphysical ϵ_{SF}. We have also concluded that if we want to decrease the inferred ϵ_{SF} below 1.0, and still have $f_b = 0.17$, we must release the c_d–M_d relation otherwise we produce a violation of the baryon conservation.

Before moving on to other possible explanations for this problem, we first examine whether this problem can be explained by the systematic uncertainties in Υ_*. As discussed in Section 3.3, in the ΛCDM framework, we expect ~10–20 per cent of Υ_{in} to be a dark-matter contribution. Reducing Υ_* by as much as 30 per cent will systematically shift all the empirical estimates of $\nabla_\ell^{obs}\Upsilon$ higher by 30 per cent (see equation 1). The R_e–M_* relation will also be affected, such that R_e for a given M_* is higher, and thus r_{in}/r_s and r_{out}/r_s in the model calculations will be higher; this leads to a higher value of $\nabla_\ell^{mod}\Upsilon$ predicted by the models which roughly offsets the higher values in the data. The final effect is for the data values of M_* to shift, and so the net change is for the low-mass galaxy data points in Fig. 7 to shift roughly parallel to the contours of constant ϵ_{SF} – not affecting the conclusions on ϵ_{SF} significantly (see Fig. 11). To decrease the inferred ϵ_{SF} for the intermediate-mass galaxies to values below 1.0 would require a dark mass fraction inside R_e of $\gtrsim 50$ per cent. Such high central dark-matter fractions are not supported by other empirical studies of the central mass content of early-type galaxies (Gerhard et al. 2001; Rusin, Kochanek & Keeton 2003). They would also imply that the average stellar M/L, $\Upsilon_{B,*} = 6.5 \pm 2.0$, must be decreased by a factor of 2: this is not plausible from the standpoint of stellar populations modelling where $\Upsilon_{B,*} \lesssim 4$ only for fairly young stellar populations, with age $\lesssim 5$ Gyr, and metallicity $-0.5 < $ [Fe/H] < 0.5 (Worthey 1994; Maraston 1998).

One way to avoid the problem of low-mass haloes is to relax the c_d–M_d relation, using a maximum plausible value of ϵ_{SF} as a prior. Once ϵ_{SF} and M_* are fixed, the total dark-halo mass, M_d, is set and the only way to alter $M_d(r)$ (equation 9) is by altering c_d. In this
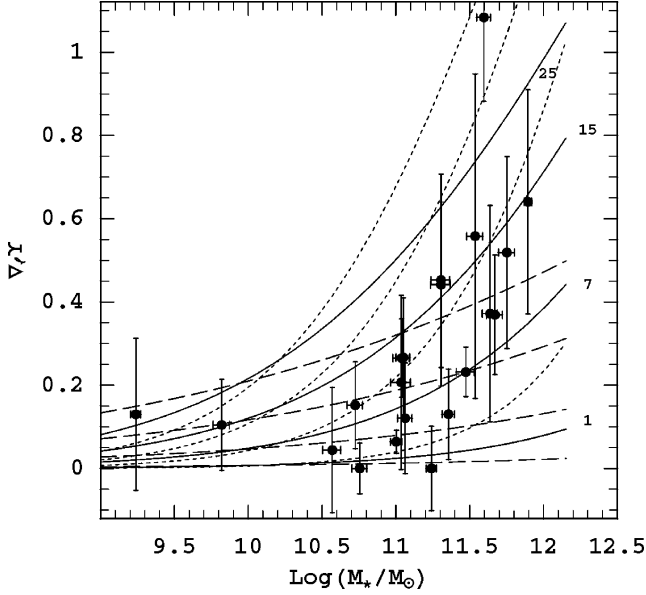
Figure 12. M/L gradients versus total luminous mass and concentration parameter after c_d–M_d relation relaxed for $\epsilon_{SF} = 0.25$. Labelled solid lines are the predictions from the ΛCDM for different c_d: line styles as in Fig. 7.

way $\nabla_\ell^{mod}\Upsilon$ can be written as a function of M_* and c_d: in Fig. 12 this is shown for $\epsilon_{SF} = 0.25$ ($f_d = 19.5$). We can derive the best-fitting c_d values for each galaxy using the same procedure adopted for best-fitting ϵ_{SF} (as in the previous section).

The results are in Fig. 13 (*left*): we see that the most massive galaxies ($M_d \sim 8 \times 10^{12}\,M_\odot$) have concentrations consistent with ΛCDM expectations ($c_d \sim 8$–14), while many of the less massive galaxies ($M_d \sim 2 \times 10^{12}\,M_\odot$) have very low concentrations ($c_d \sim 1$–6).
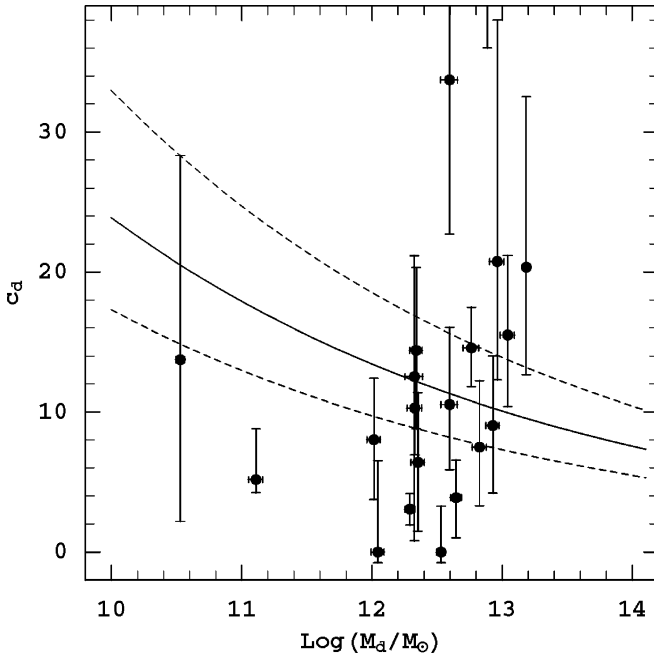
The shallow M/L gradients in the low-mass galaxies are thus a simple consequence of a small fraction of the dark matter residing in the galaxy centre. This explanation was advanced in Romanowsky et al. (2003) but contradicts ΛCDM expectations that c_d is decreasing with M_d rather than increasing. As suggested by Section 5.1, ϵ_{SF} may not be constant but rather decreasing with galaxy mass, which may alleviate the problem. We thus assume $\epsilon_{SF} = 0.25$ for $M_* > M_0$ and $\epsilon_{SF} = 1.0$ for $M_* < M_0$ (a maximum plausible value), and plot the results for c_d in Fig. 13 (*right*). The c_d–M_d relation is now in a better agreement with the ΛCDM expectation, but the low-mass galaxies still have haloes with concentrations which are too low on average.

The above alternatives (baryon non-conservation; low concentrations) for producing low M/L gradients are necessitated by the strict NFW functional form $M_d(r)$ for the haloes (equation 9). Thus there is little flexibility to change $M_{d,out}$ versus $M_{d,in}$. But another way to reduce $\nabla_\ell\Upsilon$ in the models (equation 2) is to change the ratio of $M_{d,out}$ versus $M_{d,in}$ by changing the form of the mass profile $M_d(r)$. For example, in the classic adiabatic contraction model of galaxy formation, the collapse of the baryons drags dark matter inward; this will increase $M_{d,in}$ above the nominal NFW halo central mass and decrease the inferred $\nabla_\ell^{obs}\Upsilon$. Again, the implications of this alternative would be that many other studies of central DM density are incorrect, and that the population synthesis models have overestimated Υ_* by ~ 50 per cent. As mentioned in Section 3.2, it is not clear that this adiabatic contraction scenario is really to be expected, and we leave examination of the details to a future study – but comparing the alternatives, it seems this may be the most likely one for 'saving' ΛCDM.

Of course, the ΛCDM theory is not as readily falsifiable as may be supposed, as various modifications to its simplest outline have been proposed to solve various problems. One may assume a different initial power spectrum and in principle partly solve the problems seen here; it has also been suggested that $\sigma_8 \sim 0.75$ is a reasonable
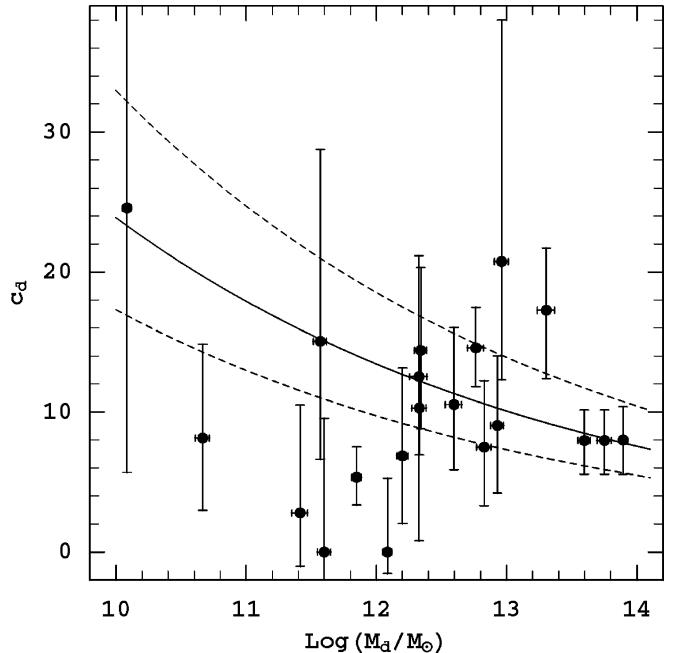

Figure 13. Best-fitting c_d values after relaxing the c_d–M_d relation for $\epsilon_{SF} = 0.25$ (left) and ϵ_{SF} varying within the galaxy sample (right: see details in the text). Solid line is c_d–M_d from B01 with 1-σ scatter indicated by dashed lines.

solution to the low-concentration halo problem (McGaugh, Barker & de Blok 2003; van den Bosch, Mo & Yang 2003).

5.3 Comparison with other dynamical techniques

For the sake of completeness, in this paragraph we briefly discuss how the results based on stellar kinematics plus PNe and GCs compare with results listed in the literature based on the techniques we have excluded in this paper: namely X-rays, gravitational lensing and H I rings. This is to verify whether (regardless of any possible selection effects) different techniques give consistent results for the dependence of the M/L gradients on stellar mass and luminosity, which we have explained as a trend of the star formation efficiency with the same global quantities.

5.3.1 X-rays

O'Sullivan & Ponman (2004b) reviewed literature results on M/L estimates based on X-ray emissions in early-type galaxies. They found that at 5–6 R_e different modelling techniques give a lower limit of $M/L = 20$ $M_\odot/L_\odot$ on a large galaxy sample. Even if most of these estimates come from cluster and group dominant galaxies, they concluded that ellipticals can possess dark haloes of their own, regardless of their environment. We can infer a lower limit for the $\nabla_\ell^{\mathrm{obs}} \Upsilon$ for these systems using their results. We can assume a $\Upsilon_{\mathrm{in}} = 7$ as the average value found in our sample and derive $\nabla_\ell^{\mathrm{obs}} \Upsilon$ (Xrays) $\geqslant 0.4$. As $M_B \lesssim -20.5$ in the X-rays sample, this is consistent with $\epsilon_{\mathrm{SF}} \lesssim 0.25$ found for our galaxy sample of stellar masses $M_* > M_0$.

5.3.2 Strong gravitational lensing

There are only a few studies where M/L of the innermost and outer regions are available for reliable $\nabla_\ell^{\mathrm{obs}} \Upsilon$ estimates. As discussed already, there is the further complication that SGL analyses refer to high z ($z \geqslant 0.1$) and they cannot be directly compared to model predictions obtained in the local universe ($z = 0$) as both dark and luminous matter scaling relations change with redshift. A detailed model prediction at high z is beyond the purpose of this paper. Here we want to give only a qualitative interpretation of SGL results.

Treu & Koopmans (2004) reviewed five bright ($M_B \lesssim -20.5$) E/S0 systems with reliable M/L estimates inside the Einstein radius (ranging from 0.8 to $5R_e$). Using their results we compute $\nabla_\ell^{\mathrm{obs}} \Upsilon \geqslant 0.4$ and an average $\nabla_\ell^{\mathrm{obs}} \Upsilon$ (SGL) ~ 0.8. These values are consistent with but somewhat higher than our dynamical results for bright galaxies, and comparison to $z = 0$ models implies a very low star formation efficiency ($\epsilon_{\mathrm{SF}} \lesssim 0.1$).

Rusin et al. (2003) used statistical constraints on the mass profiles of 22 lens systems over a broad range of luminosities to find a typical homologous mass profile. Their results (assuming a ΛCDM dark-matter profile) imply $\nabla_\ell \Upsilon \sim 0.1 - 0.2$, which is consistent with our results for faint galaxies but apparently not consistent with the Treu & Koopmans (2004) results and with our bright galaxy results. A more careful examination of these results, including treatment of the z dependence of the models, awaits a future paper.

5.3.3 H I rings

For these galaxies, the gradient prediction should account for the presence of the gas as its mass contribution it is not negligible for these systems. For the sake of simplicity, as a first approximation

we use our predictions obtained without gas as a reference. There are a few systems in the literature with reliable innermost and outer M/L values suitable for $\nabla_\ell^{\mathrm{obs}} \Upsilon$ estimates.

These galaxies include NGC 5266 (Morganti et al. 1997), IC 5063 (Morganti, Oosterloo & Tsvetanov 1998), IC 2006 (Franx, van Gorkom & de Zeeuw 1994), NGC 1052, 2974 and 4278 (Bertola et al. 1993). These galaxies span a broad range of luminosity, and we derive $\nabla_\ell^{\mathrm{obs}} \Upsilon$ values ranging from 0.4 to 1.0, corresponding to $\epsilon_{\mathrm{SF}} \lesssim 0.2$. These results are consistent with what we have found for the brighter galaxies, but the weak halo behaviour for fainter galaxies is not detected. However, as discussed earlier, we consider it dangerous to take the H I results as typical of early-type galaxies owing to selection issues.

5.4 Dwarf galaxies

In Section 3 we have made $\nabla_\ell \Upsilon$ predictions for a wide range of galaxy masses, including dwarf systems (log $M_* \lesssim 10$). This mass regime is populated by both dEs and low surface brightness late-type systems (LSBs). These two classes are different in many respects (morphology, gas content, stellar population etc.), but they also share some similarities: they are small, low-luminosity galaxies with diffuse, exponential declining surface brightness profiles.[5] Furthermore they have the same size–mass relation (Shen et al. 2003) and hence they are expected to have similar dark-to-luminous mass distributions. Specifically, as shown in Section 3.4, we must expect observed gradients to increase for decreasing stellar masses (and luminosities) and for decreasing star formation efficiency (at any given mass). Unfortunately, these galaxies remain among the most poorly studied systems, mostly because of the observational difficulties related to their faint luminosities; thus detailed dynamical analysis are scarce and generally focused on the central galaxy regions (Bender & Nieto 1990; Mateo 1998).

A complete view of these systems, although beyond the purpose of this paper, is complicated by data which are generally not suitable for the kind of analysis based on M/L gradients. Here we want to briefly compare our models with a few literature data sets which can be adapted to this analysis. We restrict our analysis to dwarf early-type galaxies which are gas poor and can be directly compared to the predictions of Section 3, where we discarded any gas component.

(i) *Fornax* (Walcher et al. 2003) [$M_B = -11.7$]: they estimate $M/L = 23$ at 90 arcmin from the galaxy centre ($R_e = 9.9$ arcmin) and a central $M/L = 4.8$. We have obtained $\nabla_\ell^{\mathrm{obs}} \Upsilon = 0.52$ for this galaxy which corresponds to $\epsilon_{\mathrm{SF}} = 0.6$ using the dwarf shallower $R_e - M_*$ relation in our models. We found consistent ϵ_{SF} values using M/L estimates from Łokas (2001).

(ii) *FS373* (De Rijcke et al. 2004) [$M_B = -16.9$]: they obtained $M/L = 7.8$ at $1.5R_e(=7.9$ arcsec/1.57 kpc) and computed a stellar $M/L = 2$–4 from age and metallicity of the stellar population. This allowed us to estimate $\nabla_\ell^{\mathrm{obs}} \Upsilon \sim 1$–2.5 and $\epsilon_{\mathrm{SF}} = 0.1$–0.6.

(iii) *FS76* (De Rijcke et al. 2004) [$M_B = -16.1$]: they obtained $M/L = 7.4$ at $1.5R_e(= 4.4$ arcsec/0.77 kpc) and considered a stellar $M/L = 2$–4 as for FS373. We found pretty similar $\nabla_\ell^{\mathrm{obs}} \Upsilon \sim 1$–2.5 but $\epsilon_{\mathrm{SF}} = 0.2$–0.45 for this galaxy.

This very preliminary test on dEs suggests that M/L gradients are actually increasing with decreasing masses as expected, and that

---

[5] In this respect our basic model assumption of an $R^{1/4}$ surface brightness profile is poorly representative for these systems.

this trend is also consistent with ϵ_{SF} tending to decrease at this mass scale from a maximum near L^*.

Low star formation efficiencies in this mass range have been also inferred for gas-rich LSB galaxies (Jobin & Carignan 1990; Cote, Carignan & Sancisi 1991; Martimbeau, Carignan & Roy 1994). They found $f_d \sim M_{tot}/M_* = 25\text{–}27^6$ in the galaxies NGC 3109, 5855 and IC 2574, respectively, corresponding to observed $\epsilon_{SF} \sim 0.2$ which are almost in agreement with efficiencies of dEs derived above. Lake, Schommer & van Gorkom (1990) claim at least half of the baryonic mass of DDO 170 in the form of gas, which implies $\epsilon_{SF} \lesssim 0.5$ assuming baryon conservation. All these ϵ_{SF} estimates are consistent with what we obtain by comparing the $\nabla_\ell^{obs}\Upsilon$ from their M/L estimates with our models (in spite of our model simplification of not including gas).

We can then conclude that, based on M/L gradients, there is evidence of low star formation efficiencies in the very low mass regime. This seems in agreement with other studies (Benson et al. 2000; Marinoni & Hudson 2002) claiming a continuous decreasing star forming efficiency with decreasing masses at these mass scales.

6 SUMMARY AND CONCLUSIONS

We have introduced a method for measuring M/L gradients in early-type (elliptical and lenticular) galaxies, quantified by $\nabla_\ell\Upsilon$. If the same technique is used for all M/L measurements in a galaxy, then $\nabla_\ell\Upsilon$ is independent of bandpass definitions and distance uncertainties. We have built typical galaxy models in the ΛCDM framework using NFW profiles for the dark-matter distribution. Assuming baryon conservation across the virial radius, these galaxies are parametrized by their total stellar mass M_* and their net star formation efficiency ϵ_{SF}; we have then made predictions for $\nabla_\ell\Upsilon$ (between $0.5R_e$ and $4R_e$) as a function of (M_*, ϵ_{SF}). As a consequence of the relative spatial scaling relations of the luminous and dark matter, we have found that brighter galaxies should typically show higher values of $\nabla_\ell\Upsilon$ than fainter ones, *appearing* more dark-matter dominated even though the overall dark-to-luminous mass fraction f_d is a constant. These predictions are valid for a mean set of galaxies only, and should not be used to draw direct conclusions about individual galaxies, whose properties are subject to considerable scatter.

We have next assembled a set of M/L measurements (using stellar, PNe and GC kinematics) in 21 early-type galaxies as a pilot study for comparing to our model predictions. We have found that $\nabla_\ell\Upsilon$ in these galaxies increases with M_* (and with other correlated parameters), which is evidence for systematic changes in either the fraction of dark matter or in its radial distribution. This empirical trend must be explained by any successful model of galaxy properties and formation (including those advocating alternative theories of gravity). Environmental density does not appear to play a key role in producing these trends.

Comparing the empirical $\nabla_\ell\Upsilon$ values to the ΛCDM predictions, we find a stellar mass scale $M_0 \sim 1.6 \times 10^{11}\,\mathrm{M}_\odot$, and a corresponding luminosity scale of $M_B \sim -20.5$, marking a galaxy dichotomy. The brighter (more massive) galaxies ($M_B \lesssim -20.5$) show a broad scatter in ϵ_{SF}, but are generally consistent with $\epsilon_{SF} \sim 0.25$. The fainter (low-mass) galaxies are generally only consistent with $\epsilon_{SF} \sim 2\text{–}3$, which is not physically possible in the context of our model assumptions.

The brighter galaxies thus appear consistent with the ΛCDM picture without need for further complications from baryonic effects.

For the fainter galaxies, we have examined some possibilities for explaining their apparent extremely high ϵ_{SF} values (i.e. apparent extremely low dark-matter fractions). One explanation is that the baryon fraction has not been conserved in these galaxies: either they have acquired large quantities of extra baryons from inflows across the virial radius (e.g. gas from nearby starbursting galaxies, which has since formed new stars); and/or they have lost portions of their outer dark haloes (after star formation) through dynamical interactions with other galaxies and groups. We note that the latter process is implicitly included in ΛCDM simulations of dark halo formation, but the net effect on f_d has not been explicitly studied.

Another explanation is that the predicted relation between halo mass M_d and concentration c_d in ΛCDM is wrong, and c_d tends to *increase* rather than *decrease* with M_d, with $c_d \sim 1\text{–}6$ for L^* galaxies. Similar conclusions have already been reached in studies of LSB galaxies (Alam et al. 2002; McGaugh et al. 2003), and may indicate that the dark matter is not CDM, or that the baryonic processes involved in galaxy formation have somehow caused the dark haloes to become less centrally concentrated. However, the current best guess for baryonic effects is that the cooling and collapse of the gas causes the dark-matter halo to also contract adiabatically (Blumenthal et al. 1986; Gnedin et al. 2004), which *increases* the central density of the halo. This is still a viable scenario for the fainter early-type galaxies if the stellar M/L values are systematically lower by 50 per cent than what we have assumed, and the central dark mass fraction is $\gtrsim 40$ per cent. This possibility merits more investigation, although we note that several studies have concluded that the dark matter cannot be so dominant. Both scenarios (low-concentration haloes; low-stellar M/L) are possible ways for resolving an apparent empirical inconsistency: weak lensing and satellite dynamics studies find evidence for large amounts of dark matter inside the virial radius in L^* early types (Guzik & Seljak 2002; van den Bosch et al. 2004), while this paper suggests little dark matter inside $\sim 4\,R_e$ in similar galaxies.

Whatever the case, these data imply a dichotomy in the dark halo profiles between fainter and brighter early-type galaxies (see Section 4.3), which parallels the dichotomy already visible in the properties of their luminous bodies (Nieto & Bender 1989; Capaccioli et al. 1992; Faber et al. 1997; Graham et al. 2003; Graham & Guzmán 2003), and X-ray properties (Pellegrini 1999), and suggests markedly different formation histories for the two galaxy populations where baryon cooling efficiencies could have played a pivotal role. The comparison of data and models also supports other studies indicating that ϵ_{SF} is at a maximum for galaxies around L^* (Benson et al. 2000; Guzik & Seljak 2002; Marinoni & Hudson 2002; van den Bosch et al. 2003). Indeed, we have briefly discussed the case of dwarf/LSB galaxies and shown that there is evidence of decreasing ϵ_{SF} from their $\nabla_\ell^{obs}\Upsilon$, supporting this scenario. We do not wish to overinterpret the implications for ΛCDM at this point, because the number of fainter galaxies in the sample is not yet statistically large, and most of them are not yet modelled in enough detail to exclude the potentially important effects of radial anisotropy at large radius. But this paper highlights the importance of detailed dynamical studies of a larger sample of galaxies, where the distribution of the dark matter as well as the stars may be used as clues to the formation histories of galaxies.

---

[6] M_{lum} in their paper refers to the total baryonic matter $M_{(stars+gas)}$.

REFERENCES

Alam S. M. K., Bullock J. S., Weinberg D. H., 2002, ApJ, 572, 34

Arnaboldi M. et al., 1996, ApJ, 472, 145 (A96)

Arnaboldi M., Freeman K. C., Gerhard O., Matthias M., Kudritzki R. P., Méndez R. H., Capaccioli M., Ford H., 1998, ApJ, 507, 759 (A98)

Baes M., Dejonghe H., 2001, ApJ, 563, L19

Bahcall N. A., Lubin L. M., Dorma V., 1995, ApJ, 447, L81

Bender R., Nieto J. L., 1990, A&A, 239, 97

Bender R., Burstein D., Faber S. M., 1992, ApJ, 399, 462

Bennett C. L. et al., 2003, ApJS, 148, 1

Benson A. J., Cole S., Frenk C. S., Baugh C. M., Lacey C. G., 2000, MNRAS, 311, 793

Bernardi M. et al., 2003, AJ, 125, 1849

Bertola F., Pizzella A., Persic M., Salucci P., 1993, ApJ, 416, L45

Blumenthal G. R., Faber S. M., Flores R., Primack J. R., 1986, ApJ, 301, 27

Borriello A., Salucci P., Danese L., 2003, MNRAS, 341, 1109

Bosma A., van der Kruit P. C., 1979, A&A, 79, 281

Bullock J. S., Kolatt T. S., Sigad Y., Somerville R. S., Kravtsov A. V., Klypin A. A., Primack J. R., Dekel A., 2001, MNRAS, 321, 559

Buote D. A., Jeltema T. E., Canizares C. R., Garmire G. P., 2002, ApJ, 577, 183

Busarello G., Capaccioli M., D'Onofrio M., Longo G., Richter G., Zaggia S., 1996, A&A, 314, 32 (B96)

Capaccioli M., Caon N., D'Onofrio M., 1992, in Danziger J., Zeilinger W. W., Kjar K., eds, ESO ESP/EIPC Workshop on Structure, Dynamics and Chemical Evolution of Early-type Galaxies (Elba). ESO, Garching, p. 43

Capaccioli M., Cappellaro E., Held E. V., Vietri M., 1993, A&A, 274, 69 (C93)

Capaccioli M., Napolitano N. R., Arnaboldi M., 2003, in Semikhatov A., Vasiliev V., Zalkin V., eds, 3rd International Sakharov Conference on Physics. (astro-ph/0211323)

Chiosi C., Bressan A., Portinari L., Tantalo R., 1998, A&A, 339, 355

Cote S., Carignan C., Sancisi R., 1991, AJ, 102, 904

Côté P., McLaughlin D. E., Cohen J. G., Blakeslee J. P., 2003, ApJ, 591, 850 (C03)

Danziger I. J., 1997, in Persic P., Salucci P., eds, ASP Conf. Ser. Vol. 117, Dark and Visible Matter in Galaxies. Astron. Soc. Pac., San Francisco, p. 28

de Blok, W. J. G., Bosma A., McGaugh S., 2003, MNRAS, 340, 657

Dekel A., Silk J., 1986, ApJ, 303, 39

De Rijcke S., Dejonghe H., Zeilinger W. W., Hau G. K. T., 2004, A&A, 426, 53

de Vaucouleurs G., 1948, Ann. d'Astrophys., 11, 247

de Zeeuw P. T. et al., 2002, MNRAS, 329, 513

Dirsch B. et al., 2004, AJ, 127, 2114

Douglas N. G. et al., 2002, PASP, 114, 1234

Dubinski J., 1998, ApJ, 502, 141

Emsellem E., Dejonghe H., Bacon R., 1999, MNRAS, 303, 495 (E99)

Faber, S. M. et al., 1997, AJ, 114, 1771

Forbes D. A., Franx M., Illingworth G. D., 1995, AJ, 109, 1988

Franx M., van Gorkom J. H., de Zeeuw T., 1994, ApJ, 436, 642

Fukugita M., Hogan C. J., Peebles P. J. E., 1998, ApJ, 503, 518

Gentile G., Salucci P., Klein U., Vergani D., Kalberla P., 2004, MNRAS, 351, 903

Gerhard O., Kronawitter A., Saglia R. P., Bender R., 2001, AJ, 121, 1936

Gebhardt K. et al., 2003, ApJ, 583, 92 (G03)

Gnedin O. Y., Kravtsov A. V., Klypin A. A., Nagai D., 2004, ApJ, 616, 16

Graham A. W., Guzmán R., 2003, AJ, 125, 2936

Graham A. W., Erwin P., Trujillo I., Asensio Ramos A., 2003, AJ, 125, 2951

Guzik J., Seljak U., 2002, MNRAS, 335, 311

Hernquist L., 1990, ApJ, 356, 359

Jimenez R., Panter B., Heavens A., Verde L., 2005, MNRAS, 356, 495

Jobin M., Carignan C., 1990, AJ, 100, 648

Kauffmann G. et al., 2003, MNRAS, 341, 33

Keeton C. R., 2001, ApJ, 561, 46

Koopmans L. V. E., Treu T., 2002, ApJ, 568, L5

Kormendy J., 1977, ApJ, 218, 333

Kronawitter A., Saglia, R. P., Gerhard, O., Bender, R. 2000, A&AS, 144, 53 (K00)

Kuntschner H., Lucey J. R., Smith R. J., Hudson M. J., Davies R. L., 2001, MNRAS, 323, 615

Lake G., Schommer, R. A., van Gorkom, J. H., 1990, AJ, 99, 547

Loewenstein M., White R. E., 1999, ApJ, 518, 50

Łokas E. L., 2001, MNRAS, 327, L21

McGaugh S. S., Barker M. K., de Blok W. J. G., 2003, ApJ, 584, 566

Magorrian, J., Ballantyne D., 2001, MNRAS, 322, 702 (MB01)

Mamon, G. A., Łokas E. L., 2004a, MNRAS, submitted (astro-ph/0405466)

Mamon G. A., Łokas E. L., 2004b, MNRAS, submitted (astro-ph/0405491)

Maraston C., 1998, MNRAS, 300, 872

Marchesini D., D'Onghia E., Chincarini G., Firmani C., Conconi P., Molinari E., Zacchei A., 2002, ApJ, 575, 801

Marinoni C., Hudson M. J., 2002, ApJ, 569, 101

Martimbeau N., Carignan C., Roy, J. R., 1994, AJ, 107, 543

Mateo M. L., 1998, ARA&A, 36, 435

Matsushita K., Belsole E., Finoguenov A., Böhringer H. 2002, A&A, 386, 77

Méndez R. H., Riffeser A., Kudritzki R.-P., Matthias M., Freeman K. C., Arnaboldi M., Capaccioli M., Gerhard O. E., 2001, ApJ, 563, 135 (M01)

Meza A., Navarro J. F., Steinmetz M., Eke V. R., 2003, ApJ, 590, 619

Mo H. J., Mao S., 2004, MNRAS, 353, 829

Moore B., Quinn T., Governato F., Stadel J., Lake G., 1999, MNRAS, 310, 1147

Morganti R., Sadler E. M., Oosterloo T., Pizzella A., Bertola F., 1997, AJ, 113, 937

Morganti R., Oosterloo T., Tsvetanov Z., 1998, AJ, 115, 915

Myers S. T. et al., 1995, ApJ, 447, L5

Napolitano N. R., Arnaboldi M., Capaccioli M., 2002, A&A, 383, 791

Napolitano N. R. et al., 2004, in Ryder S., Pisano D. J., Walker M., Freeman K. C., eds, Proc. IAU Symp. 220, Dark Matter in Galaxies. Astron. Soc. Pac., San Francisco, p. 173

Navarro J. F., Frenk C. S., White S. D., 1996, ApJ, 462, 563 (NFW)

Navarro J. F., Frenk C. S., White S. D., 1997, ApJ, 490, 493 (NFW)

Navarro J. F. et al., 2004, MNRAS, 349, 1039

Nieto J. L., Bender R., 1989, A&A, 215, 266

Oosterloo T. A., Morganti R., Sadler E. M., Vergani D., Caldwell N., 2002, AJ, 123, 729

O'Sullivan E., Ponman T. J., 2004a, MNRAS, 349, 535

O'Sullivan E., Ponman T. J., 2004b, MNRAS, 354, 935

Padmanabhan N. et al., 2004, New Astron., 9, 329

Pahre M. A., Djorgovski S. G., de Carvalho R. R., 1995, ApJ, 453, L17

Pahre M. A., Djorgovski S. G., de Carvalho R. R., 1998, AJ, 116, 1591

Pellegrini S., 1999, A&A, 351, 487

Peng E. W., Ford H. C., Freeman K. C., 2004, ApJ, 602, 685 (P04)

Press W. H., Teukolsky S. A., Vetterling W. T., Flannery B. P., 1992, Numerical Recipes in C, 2nd edn. Cambridge Univ. Press, Cambridge

Ravindranath S., Ho L. C., Peng C. Y., Filippenko A. V., Sargent W. L. W., 2001, AJ, 122, 653

Richtler T. et al., 2004, AJ, 127, 2094 (R04)

Romano D., Silva L., Matteucci F., Danese L., 2002, MNRAS, 334, 444

Romanowsky A. J., Kochanek C. S., 2001, ApJ, 553, 722 (RK01)

Romanowsky A. J., Douglas N. G., Arnaboldi M., Kuijken K., Merrifield M. R., Napolitano N. R., Capaccioli M., Freeman K. C., 2003, Sci, 301, 1696 (R03)

Rusin D., Kochanek C. S., Keeton C. R., 2003, ApJ, 595, 29

Saglia R. P., Kronawitter A., Gerhard O., Bender R., 2000, AJ, 119 153 (S00)

Sáiz A., Domínguez-Tenreiro R., Serna A., 2004, ApJ, 601, L131

Shen S., Mo H. J., White S. D. M., Blanton M. R., Kauffmann G., Voges W., Brinkmann J., Csabai I., 2003, MNRAS, 343, 978

Sommer-Larsen J., Götz M., Portinari L., 2003, ApJ, 596, 47

Statler T. S., Dejonghe H., Smecker-Hane T., AJ, 117, 126 (S99)

Terlevich A. I., Forbes D. A., 2002, MNRAS, 330, 547

Tonry J. L., Dressler A., Blakeslee J. P., Ajhar E. A., Fletcher A. B., Luppino G. A., Metzger M. R., Moore C. B., 2001, ApJ, 546, 681

Trager S. C., Faber S. M., Worthey G., González J. J., 2000, AJ, 120, 165

Tremblay B., Merritt D., Williams T. B., 1995, ApJ, 443, L5 (T95)

Treu T., Koopmans L. V. E., 2004, ApJ, 611, 739

Trujillo I., Burkert A., Bell E. F., 2004, ApJ, 600, L39

Tully R. B., 1988, Nearby Galaxies Catalog. Cambridge Univ. Press, Cambridge

van den Bosch F. C., Mo H. J., Yang X., 2003, MNRAS, 345, 923

van den Bosch F. C., Norberg P., Mo H. J., Yang X., 2004, MNRAS, 352, 1302

van der Marel R. P., 1991, MNRAS, 253, 710 (M91)

Verolme E. K. et al., 2002, MNRAS, 335, 517 (V02)

Walcher C. J., Fried J. W., Burkert A., Klessen R. S., 2003, A&A, 406, 847

Wechsler R. H., Bullock J. S., Primack J. R., Kravtsov A. V., Dekel A., 2002, ApJ, 568, 52

Weinberg D. H., Davé R., Katz N., Hernquist L., 2004, ApJ, 601, 1

Whitmore B. C., Forbes D. A., Rubin V. C., 1988, ApJ, 333, 542

Worthey G., 1994, ApJS, 95, 107

Wright L. J., Ostriker J. P., Naab T., Efstathiou G., 2003, MNRAS, submitted (astro-ph/0310513)

This paper has been typeset from a TEX/LATEX file prepared by the author.